AD-A139 125 A RAPID METHOD FOR PREDICTING SUCTION DISTRIBUTIONS TO MAINTAIN ATTACHED..(U) PENNSYLVANIA STATE UNIV UNIVERSITY PARK APPLIED RESEARCH LAB.. G H HOFFMAN

1/1

UNCLASSIFIED 09 DEC 83 ARL/PSU/TM-83-201 F/G 20/4 NL

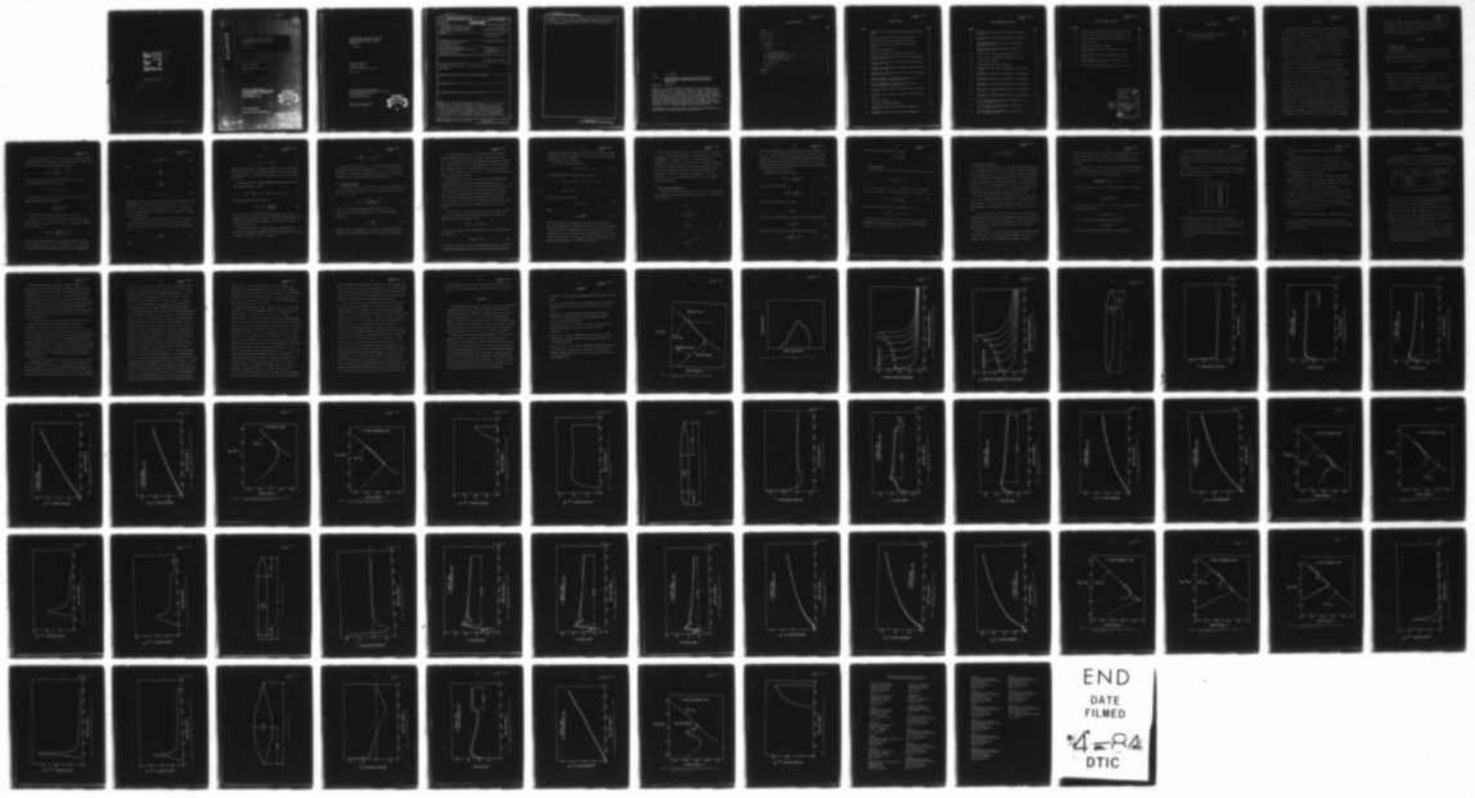

END

DATE FILMED

4-84

DTIC

A RAPID METHOD FOR PREDICTING SUCTION DISTRIBUTIONS TO MAINTAIN ATTACHED, LAMINAR BOUNDARY LAYERS ON BODIES OF REVOLUTION

G. H. Hoffman

Technical Memorandum
File No. TM 83-201
9 December 1983
Contract No. N00024-79-C-6043

Copy No. 8

The Pennsylvania State University
Intercollege Research Programs and Facilities
APPLIED RESEARCH LABORATORY
Post Office Box 30
State College, Pa. 16801

NAVY DEPARTMENT

NAVAL SEA SYSTEMS COMMAND

A RAPID METHOD FOR PREDICTING SUCTION DISTRIBUTIONS TO MAINTAIN ATTACHED, LAMINAR BOUNDARY LAYERS ON BODIES OF REVOLUTION

G. H. Hoffman

Technical Memorandum
File No. TM 83-201
9 December 1983
Contract No. N00024-79-C-6043

Copy No. 8

The Pennsylvania State University
Intercollege Research Programs and Facilities
APPLIED RESEARCH LABORATORY
Post Office Box 30
State College, PA 16801

Approved for Public Release
Distribution Unlimited

UNCLASSIFIED

SECURITY CLASSIFICATION OF THIS PAGE (When Data Entered)

REPORT DOCUMENTATION PAGE	READ INSTRUCTIONS BEFORE COMPLETING FORM
1. REPORT NUMBER: TM 83-201	2. GOVT ACCESSION NO.: A139125
3. RECIPIENT'S CATALOG NUMBER	
4. TITLE (and Subtitle): A RAPID METHOD FOR PREDICTING SUCTION DISTRIBUTIONS TO MAINTAIN ATTACHED, LAMINAR BOUNDARY LAYERS ON BODIES OF REVOLUTION	5. TYPE OF REPORT & PERIOD COVERED: Technical Memorandum
	6. PERFORMING ORG. REPORT NUMBER
7. AUTHOR(s)	8. CONTRACT OR GRANT NUMBER(s): N00024-79-C-6043
9. PERFORMING ORGANIZATION NAME AND ADDRESS: Applied Research Laboratory, Post Office Box 30, State College, PA 16804	10. PROGRAM ELEMENT, PROJECT, TASK AREA & WORK UNIT NUMBERS
11. CONTROLLING OFFICE NAME AND ADDRESS: Naval Sea Systems Command, Code NSEA 63R-12, Department of the Navy, Washington, DC 20362	12. REPORT DATE: 9 December 1983
	13. NUMBER OF PAGES: 75
14. MONITORING AGENCY NAME & ADDRESS (if different from Controlling Office)	15. SECURITY CLASS (of this report)
	15a. DECLASSIFICATION DOWNGRADING SCHEDULE

16. DISTRIBUTION STATEMENT (of this Report)

Approved for public release. Distribution unlimited.
Per NAVSEA -

17. DISTRIBUTION STATEMENT (of the abstract entered in Block 20, if different from Report)

18. SUPPLEMENTARY NOTES

19. KEY WORDS (Continue on reverse side if necessary and identify by block number)

of A.M.O. Smith's procedure

20. ABSTRACT (Continue on reverse side if necessary and identify by block number)

An approximate method is presented for the determination of the minimum amount of suction necessary to maintain a laminar, attached boundary layer in incompressible, axisymmetric flow. The method is an extension of a procedure due to A. M. O. Smith which calculates a general laminar boundary layer by piecewise similarity solutions. The extension has been programmed on a VAX 11/782 computer and found to be extremely fast, taking from 3 to 4 secs. in CPU time. Boundary-layer solutions for four

DD FORM 1 JAN 73 1473 EDITION OF 1 NOV 65 IS OBSOLETE

UNCLASSIFIED

SECURITY CLASSIFICATION OF THIS PAGE (When Data Entered)

(cont)

axisymmetric bodies at a variety of Reynolds numbers have been obtained and the results are compared with finite difference solutions which use the suction distribtuion from the approximate theory. Agreement between the two is generally good.

From: G. H. Hoffman

Subject: A Rapid Method for Predicting Suction Distributions to Maintain Attached, Laminar Boundary Layers on Bodies of Revolution

References: See Page 28

Abstract: An approximate method is presented for the determination of the minimum amount of suction necessary to maintain a laminar, attached boundary layer in incompressible, axisymmetric flow. The method is an extension of a procedure due to A. M. O. Smith which calculates a general laminar boundary layer by piecewise similarity solutions. The extension has been programmed on a VAX 11/782 computer and found to be extremely fast, taking from 3 to 4 secs. in CPU time. Boundary-layer solutions for four axisymmetric bodies at a variety of Reynolds numbers have been obtained and the results are compared with finite difference solutions which use the suction distribution from the approximate theory. Agreement between the two is generally good.

Acknowledgment: This work was supported by the Systems Technology Branch of the Undersea Warfare Technology Office (NAVSEA 63R-12).

--

TABLE OF CONTENTS

9 December 1983
GHH:lhm

LIST OF FIGURES

LIST OF FIGURES (continued)

--

LIST OF FIGURES (continued)

--

LIST OF TABLES

1. INTRODUCTION

In performing parametric design studies on underwater bodies where the flow properties of the boundary layer are required, a fast-running procedure to calculate those properties is a must. Another requirement of the boundary-layer calculation procedure is reasonable accuracy. Finite difference procedures can be ruled out because they require too much computer time. Thus the choice must be made from the numerous fast running but less accurate approximate methods which are based on simplified forms of the boundary-layer equations such as integral methods or local similarity methods, c.f. Chapter 6 of Rosenhead [1].

The particular aspect of the boundary-layer problem addressed here is the determination of the suction distribution required to maintain laminar, attached flow in the axisymmetric, incompressible case. As a rapid and rasonably accurate means of solving this problem the local similarity approach was chosen. Walz in 1941 [2] was the first to use this approach as a means of solving the integral form of the momentum equation. In this method the velocity profile is represented by a self-similar wedge flow profile where the similarity variables are related to the general external flow variables. The advantage of this method is that it can be used in regions of very rapid pressure drop where the methods based on polynomial profiles, such as that of Pohlhausen, break down. In 1956 Smith [3] advanced a method very similar to that of Walz based on piecewise wedge flow solutions over finite intervals in body arc length. Smith's method becomes identical to Walz's method as the arc length shrinks to zero. Smith applied his procedure to a variety of two-dimensional and axisymmetric cases without suction and found the accuracy to be comparable to any of the integral methods. His method has the advantage

of being very simple to apply and can easily be extended to boundary layers with suction. This report presents the extension of Smith's method to the particular case where the amount of suction is determined by the critical Reynolds number (neutral stability) curve.

2. ANALYSIS

2.1 The Method of Smith

Smith's method rests on the assumption that a general incompressible laminar boundary layer solution can be closely approximated by a piecewise matching of Falkner-Skan similarity solutions for wedge flows. The analysis starts with the wedge flow surface speed expression

$$u_e = k(x - x_o)^{\frac{\beta}{2-\beta}} , \qquad (1)$$

where u_e is the inviscid surface speed, x_o is the arbitrary origin, k is a constant, β is the Falkner-Skan pressure gradient parameter, or Hartree parameter and x in the present context is body arc length.

Equation (1) is matched to the actual surface speeds at Points 1 and 2 of an arbitrary interval $x_1 \leq x \leq x_2$. This matching yields the two relations:

$$u_{e_1} = k(x_1 - x_o)^{\frac{\beta}{2-\beta}} , \qquad (2)$$

$$u_{e_2} = k(x_2 - x_o)^{\frac{\beta}{2-\beta}} , \qquad (3)$$

where u_{e_1} and u_{e_2} are the surface speeds from the actual distribution.

The second assumption, based on physical grounds, is that the momentum thickness given by the piecewise wedge flow solutions must be continuous. The wedge flow relation for the actual momentum thickness θ is

$$\theta \, Re^{1/2} = \left[\left(\frac{x-x_o}{u_e}\right)(2-\beta)\right]^{1/2} \hat{\theta} \quad , \tag{4}$$

where Re is the Reynolds number based on body axial length, $\hat{\theta}$ is the self-similar momentum thickness defined by,

$$\hat{\theta} = \int_o^\infty (1 - f')f' d\eta \quad , \tag{5}$$

f is the solution of the Falkner-Skan differential equation and η is the wedge flow similarity variable defined by

$$\eta = \left[\frac{Reu_e}{(x-x_o)(2-\beta)}\right]^{1/2} y \quad . \tag{6}$$

The prime in Eq. (5) denotes differentiation with respect to η.

Equations (2) and (3) are two relations for the determination of the three constants x_o, k and β. The third relation is obtained by evaluating Eq. (4) at Point 1, viz,

$$\theta_1 \, Re^{1/2} = \left[\left(\frac{x_1-x_o}{u_{e_1}}\right)(2-\beta)\right]^{1/2} \hat{\theta} \quad , \tag{7}$$

and θ_1 is known from calculations on the preceding interval. The only quantity needed of the three is β. By eliminating x_o and k, one obtains the following transcendental equation for β (see Ref. 3 for the details):

$$\left[1 + (2 - \beta)\hat{\theta}^2 Z\right]^{\frac{\beta}{2-\beta}} = 1 + \phi \quad , \tag{8}$$

where

$$\phi = \frac{u_{e_2} - u_{e_1}}{u_{e_1}} \quad , \tag{9}$$

$$Z = \frac{x_2 - x_1}{\theta_1 \cdot Re_{\theta_1}} \quad , \tag{10}$$

$$Re_{\theta_1} = Re \cdot u_{e_1} \cdot \theta_1 \quad . \tag{11}$$

The parameters ϕ and Z are known from the body surface speed distribution and the boundary-layer calculations from the preceding step. In Eq. (8), $\hat{\theta}$ is a function of β which requires the Falkner-Skan solutions to be known and an interpolation scheme to be used to determine $\hat{\theta}$. The interpolation procedure will be discussed later.

Two methods are available for the solution of Eq. (8) for β. The first involves an iteration formula obtained by taking the natural logarithm of both sides of Eq. (8) and solving for β outside the logarithm. This formula is:

$$\beta = \frac{2a}{a+b} \quad , \tag{12}$$

where

$$a = \ell n(1 + \phi) \quad , \tag{13}$$

$$b = \ell n\left[1 + (2 - \beta)\hat{\theta}^2 Z\right] \quad . \tag{14}$$

Equation (12) has excellent convergence properties for $\beta > 0$, converging to four decimal places in β in four to six iterations. For $\beta < 0$, successive approximations to β oscillate but still converge, only at a slower rate than for $\beta > 0$.

The second method is a straightforward Newton procedure where the root of the following equation is sought:

$$F(\beta) = \frac{\beta}{2-\beta}\, \ell n\left[1 + (2 - \beta)\hat{\theta}^2 Z\right] - \ell n(1 + \phi) = 0 \quad . \tag{15}$$

Then successive iterates for β are given by

$$\beta^{(n+1)} = \beta^{(n)} - \left[\frac{F(\beta)}{F'(\beta)}\right]^{(n)} \quad . \tag{16}$$

In Eq. (16) superscript n denotes the iteration number and F' is the derivative of F with respect to β which is most easily determined numerically. Equation (15) has been found to converge in all cases tried and in fewer iterations than Eq. (12).

With β known, θ_2 must be computed to continue the boundary-layer calculation. The formula is obtained from Eq. (4) with the help of Eqs. (2), (3) and (7) to eliminate k and x_o. The result is

$$\theta_2 = \left\{ \frac{u_{e_1}}{u_{e_2}} \left[1 + (2 - \beta)\hat{\theta}^2 Z \right] \right\}^{1/2} \theta_1 \quad . \tag{17}$$

Note that over the interval $x_1 \leq x \leq x_2$, the Falkner-Skan quantities β and $\hat{\theta}$ (and hence $\hat{\delta}^*$ and H) are constant. Thus β, $\hat{\theta}$, $\hat{\delta}^*$ and H have a stair-step behavior. Consequently the physical δ^* and H also have a discontinuous behavior with only θ being smooth because it was forced to be.

2.2 Extension to Suction

The extension of Smith's method to include suction is straightforward and begins with the wedge flow formula for v_w, the velocity normal to the surface (c.f. Ref. 1, p. 235),

$$Re^{1/2} v_w = - \left[\frac{u_e}{(x-x_o)(2-\beta)} \right]^{1/2} f_w \quad , \tag{18}$$

where f_w is the similarity stream function evaluated at the wall. Equation (4) can be used to eliminate x_o in Eq. (18) giving the more useful form:

$$v_w = - \frac{\hat{\theta} f_w}{\theta Re} \quad . \tag{19}$$

Because $\hat{\theta}$ and f_w are constants in an interval, v_w will be discontinuous at interval junctions but this behavior will not turn out to be a hindrance.

In the present application just the right amount of suction must be applied so that small disturbances in the laminar boundary layer will not grow. The neutral stability curve then becomes the constraint that determines v_w. As shown by Wazzan et al [4], neutral stability calculations for a wide range of boundary-layer flows, when plotted as $(Re_\delta^*)_{crit}$ versus the shape factor H, form a single curve -- see their Fig. 1. This curve in tabular form is used as the constraint relation.

As illustrated in Fig. 1, for a given body the path of boundary-layer development (Re_δ^* versus H) with no suction proceeds upward toward the critical curve as the distance from the stagnation point increases. The point of intersection of the path with the critical curve is where suction must begin. From the intersection onward the path is constrained to follow the critical curve and thus determines the minimum suction distribution to maintain laminar flow. Once suction is turned off the path immediately leaves the critical curve and transition or laminar separation or both follows quickly.

On each interval on the body beginning at the nose the Reynolds number based on δ^* is calculated and tested against $(Re_\delta^*)_{crit}$ determined from Wazzan's relation for the given H. Then if

$$(Re_\delta^*)_{calc} > (Re_\delta^*)_{crit} \quad ,$$

the constraint relation is invoked to determine β and f_w. This relation can be written as

$$(Re_\delta^*)_{calc} = W(H) \quad , \tag{20}$$

where W(H) is the Wazzan et al critical Reynolds number relation. Since the calculated boundary-layer quantities have been found to show insignificant

--

differences with regard to where Re_δ^* is computed in each interval, provided the interval is small, the beginning point of the interval is chosen because the calculation of β is simplified.

Equation (20) is therefore written as

$$(Re_\delta^*)_1 = W(H) \quad . \tag{21}$$

The displacement thickness Reynolds number is given by

$$(Re_\delta^*)_1 = Re \cdot u_{e_1} \cdot \delta_1^* = Re \cdot u_{e_1} \cdot \vartheta_1 \cdot H$$

$$(Re_\delta^*)_1 = Re_{\vartheta_1} \cdot H \quad .$$

Then Eq. (21) can be rewritten as

$$Re_{\theta_1} = G(H) \quad , \tag{22}$$

where

$$G(H) = \frac{W(H)}{H} \quad . \tag{23}$$

Equation (22) shows why the beginning of the interval was chosen. Since Re_{θ_1} is known (because θ is continuous and hence so is Re_θ), Eq. (22) provides a means for the direct determination of H by interpolation of the relation of Wazzan et al. Thus the iteration for β is performed along an H = constant line which eliminates f_w as an independent parameter, as will be seen. The equation that determines β is, of course, still Eq. (8).

Once β is known for the interval, θ_2 is computed from Eq. (17) and then v_{w_1} and v_{w_2} are computed from Eq. (19). As illustrated in Fig. 2, the typical v_w distribution, as given by Eq. (19), has a saw-tooth character. A continuous suction distribution is usually desired for design purposes as well as for finite difference calculations to verify the approximate results. The best agreement between approximate and finite difference boundary-layer calculations was found for a "continuous" distribution of v_w versus x consisting of $(v_w)_{min}$ at the segment junction points, i.e., the largest suction speed magnitude.

2.3 Axially Symmetric Formulation

The preceding derivation, as Smith shows, can readily be extended to the axially symmetric case by use of the Mangler transformation. The form used by Smith is as follows:

$$\left.\begin{aligned} \tilde{u}_e &= u_e \\ \tilde{x} &= \int_o^x \left(\frac{r_o}{R}\right)^2 dx \\ \tilde{y} &= \frac{r_o}{R}\, y \\ \tilde{\beta} &= \beta \\ \tilde{v}_w &= \frac{R}{r_o}\, v_w \end{aligned}\right\} \qquad (24)$$

where barred quantities denote the transformed equivalent two-dimensional flow, y is distance normal to the body, r_o is body radius and R is maximum body radius. Then in the wedge flow relations all physical variables are replaced by their barred equivalents which follows from the fact that the axially symmetric boundary-layer equations transform into a two-dimensional form via the Mangler transformation.

By definition, the momentum area is,

$$\bar{\theta} = \int_o^\infty \left(1 - \frac{u}{u_e}\right) \frac{u}{u_e} \frac{r_o}{R} \, dy \quad , \tag{25}$$

and the 2-D momentum thickness is,

$$\theta = \int_o^\infty \left(1 - \frac{u}{u_e}\right) \frac{u}{u_e} \, dy \quad . \tag{26}$$

The two are therefore related as follows:

$$\bar{\theta} = \frac{r_o}{R} \theta \quad . \tag{27}$$

Similarly, the displacement area is related to the displacement thickness by,

$$\bar{\delta}^* = \frac{r_o}{R} \delta^* \quad . \tag{28}$$

Then in terms of $\bar{\theta}$ the critical Reynolds number relation becomes

$$Re_{\bar{\theta}_1} \left(\frac{R}{r_o}\right)_1 = G(H) \quad , \tag{29}$$

--

and the expression for suction velocity reads

$$v_w = -\frac{r_o}{R} \cdot \frac{\hat{\theta}}{\bar{\theta}} \frac{f_w}{Re} \quad . \tag{30}$$

2.4 Starting Solution

In the vicinity of the stagnation point on a blunt body, the relation for $\bar{\theta}$ is

$$\bar{\theta}^2 \, Re = \frac{\bar{x}}{\bar{u}_e} (2 - \bar{\beta}) \hat{\theta}^2 \quad . \tag{31}$$

At the stagnation point $\bar{x} = 0$ and $\bar{u}_e = 0$; hence Eq. (31) is indeterminate. Thus $\bar{\theta}$ at the stagnation is obtained as the limit of Eq. (31) as $\bar{x} \to 0$, viz.

$$\bar{\theta}_{sp} = 0.4285 \left[Re \left(\frac{d\bar{u}_e}{d\bar{x}} \right)_{sp} \right]^{-1/2} \quad , \tag{32}$$

where the values used for $\bar{\beta}$ and $\hat{\theta}$ at the stagnation point are:

$$\bar{\beta}_{sp} = 0.5 \; , \; \hat{\theta}_{sp} = 0.3499 \quad .$$

Equation (31) must also be used to determine $\bar{\theta}$ at the first station downstream of the stagnation point, $\bar{x} = \bar{x}_2$, because the general procedure using Eqs. (2), (3) and (7) is invalid. Thus

--

$$\bar{\theta}_2 = 0.4285 \left(\frac{\bar{x}_2}{Re \cdot \bar{u}_{e_2}} \right)^{1/2} . \qquad (33)$$

2.5 Automation of the Method

The original Smith method was set up for graphical solution using plots of the Falkner-Skan solution ($f_w = 0$) in the form of Λ versus β for constant values of Z, where $\Lambda = \phi/Z$. For solution by digital computer, the parameter ϕ is more convenient and the graphs must be replaced by a large data base of Falkner-Skan solutions. The parameters chosen for the data base were H and $\hat{\delta}^*$ versus β and f_w, including the separation values. The ranges covered in β and f_w are $-2.0 \leq \beta \leq 2.0$ and $0 \leq f_w \leq 2.5$ which has been found to be adequate for almost all the numerical examples considered to date.

The curves of H and $\hat{\delta}^*$ versus β for constant values of f_w are shown in Figs. 3 and 4. Each of these plots is represented in the data base by 227 discrete values. The data base also contains the Wazzan et al critical Reynolds number curve represented by 11 points for β in the range 2.0 to 3.0.

To obtain the values of H and $\hat{\delta}^*$ for the data base, the Falkner-Skan differential equation was solved numerically, for β and f_w given, using the method of Keller [5]. Double precision arithmetric was used and each profile was represented by 50 intervals in the similarity variable η spaced in a geometric progression.

The upper limit $\beta = 2$ in the data base corresponds to the maximum value possible for wedge flow solutions for which the wedge half angle is 180 degrees. Above $\beta = 2$, the present method breaks down. In certain

applications, notably for flat nose bodies, β will exceed 2 but the region in x over which this occurs is usually small. Thus setting $\beta = 2$ in such a region produces a negligible error in the present method, as noted by Smith.

The condition $\beta > 2$ will always occur close to the nose before suction is applied. The occurrence of $\beta = 2$ can be detected by a relation derived from Eq. (8). If Eq. (8) is written in the following form:

$$\frac{\ell n[1+\hat{\theta}^2 Z\cdot(2-\beta)]}{2-\beta} = \frac{1}{\beta}\,\ell n\,(1+\phi) \quad , \tag{34}$$

then the left-hand side is seen to be indeterminate when $\beta = 2$. By letting $\varepsilon = 2 - \beta$, then

$$\lim_{\varepsilon\to 0} \frac{\ell n(1+\hat{\theta}^2 Z\varepsilon)}{\varepsilon} = \hat{\theta}^2 Z$$

and noting that for $\beta = 2$ and $f_w = 0$, $\hat{\theta} = 0.2279$, the final limiting form of Eq. (34) is found to be,

$$Z = 9.6246\ \ell n(1+\phi) \quad .$$

For $\beta < 2$, the following inequality must therefore hold:

$$Z > 9.6246\ \ell n(1+\phi) \quad . \tag{35}$$

Thus, whenever this inequality is violated β is set to equal to 2.

For a particular approximation to β in the solution of Eq. (8), for given Z and ϕ, $\hat{\theta}$ is obtained from interpolated values of H and $\hat{\delta}^*$. These latter two quantities are determined by quadratic Lagrange interpolation. For the no suction case ($f_w = 0$) the tables of H and $\hat{\delta}^*$ are merely interpolated for the given β.

For the case $f_w > 0$, H is first determined by linear interpolation of the Wazzan et al critical Reynolds number curve using $\log_{10} G$. The values of $\log_{10} G$ versus H are given in Table 1.

H	$\log_{10} G$
2.0	4.362
2.1	4.093
2.2	3.814
2.3	3.478
2.4	3.110
2.5	2.702
2.6	2.305
2.7	2.037
2.8	1.863
2.9	1.716
3.0	1.623

Table 1. Critical Reynolds Number Values of Wazzan et al.

The interpolation procedure to obtain $\hat{\delta}^*$ and f_w is as follows:

(1) Interpolate each f_w = constant curve in the data base to obtain values of β and $\hat{\delta}^*$ for the given H. This process produces curves of $\hat{\delta}^*$ versus β and f_w versus β for H = constant.

(2) For the given β, interpolate the curves from Step 1 to obtain $\hat{\delta}^*$ and f_w.

--

We note that f_w is actually not needed until the β calculation has converged.

The Falkner-Skan curves of H versus β and $\hat{\delta}^*$ versus β, with f_w = constant, in the region $\beta < 0$ and $f_w > 0$ end at the separation point with an infinite slope. In this region interpolation along H = constant lines is actually a much more accurate way to determine f_w and $\hat{\delta}^*$ (for a given β) than interpolating on β = constant lines.

The determination of β and f_w, as dictated by the critical Reynolds number curve, will automatically preclude the occurrence of separation. The reason is that as the critical Reynolds number increases, H must decrease and will always be less than the corresponding separation value.

If suction is turned off, H will increase very rapidly and transition will ensue. To detect this occurrence the correlation of Wazzan et al for Re_x versus H is used. The Reynolds number is based on the body arc length, as measured from the stagnation point, of the point where a disturbance amplification ratio of e^9 occurs. This correlation has been found by Wazzan et al to be fitted closely by the equation:

$$\log_{10}\left[Re_x(e^9)\right] = -40.4557 + 64.8066H - 26.7538H^2 + 3.3819H^3 \quad . \quad (36)$$

If Re_x at the particular point on the body is found to be greater than $Re_x(e^9)$ from Eq. (36), then transition has taken place and the boundary-layer calculation is stopped.

3. NUMERICAL RESULTS

Suction distributions, as well as boundary layer integral properties, have been computed for four different body shapes at Reynolds numbers ranging from 10^6 to 10^8. Table 2 gives the particular Reynolds numbers for each case.

Case	Body Shape	Reynolds Numbers
1	Laminar Flow Body in Tunnel	10^6, 10^7
2	NSRDC Body	10^6, 10^7
3	Flat Nose Body	10^6, 10^7, 10^8
4	F-57 Body	1.2×10^6

Table 2. Body Shapes and Reynolds Numbers.

These particular bodies were chosen because each pressure distribution is significantly different. Case 1 has no adverse pressure gradient near the nose, Case 2 has a mild adverse pressure gradient near the nose, Case 3 has a very strong adverse pressure gradient near the nose and Case 4 has a medium strength adverse pressure gradient near its mid-section. In both Cases 3 and 4 the adverse pressure gradient is strong enough to cause separation of the laminar boundary layer without suction. These two cases provide the most severe test of the approximate theory.

To verify the approximate theory, the "smoothed" suction distribution, described in Section 2.2, was input to a finite difference code based on Keller's Box Method and the laminar boundary-layer properties calculated. The finite difference results, which can be considered exact, were then compared with their approximate counterparts.

Numerical results for the approximate theory were obtained on a VAX 11/782 computer using single precision arithmetric. Typical CPU times ranged between 3 and 4 seconds whereas the corresponding finite difference solutions took between 27 and 35 seconds in CPU, a factor of 9 increase. The step size distributions along the bodies studied were governed by the accuracy requirements of both the inviscid solutions, from which the pressure distributions were obtained, and the finite difference boundary-layer solutions. The number of points along the bodies used in the boundary-layer calculations (approximate and exact) ranged from 73 to 88 over a total arc length range of 0.63 to 0.72.

Body geometry and inviscid surface pressure distribution are given for each case. Then comparisons of approximate results are given for distributions of shape factor H and momentum area $\bar{\theta}$. For the finite difference results, the path of development of the boundary layer is given in terms of $\log_{10}(Re_{\delta}^{*})$ versus H, and finally, the suction velocity distribution from the approximate theory is given. The most significant of the above as a means of judging the worth (accuracy) of the approximate theory is the path of boundary-layer development. The closeness with which the finite difference results follow the critical Reynolds number curve as a result of suction is a measure of the accuracy of the approximate theory to predict the correct suction distribution.

Results for the laminar flow body in tunnel are shown in Figs. 5 through 14. The body geometry appears in Fig. 5 and the pressure distribution in Fig. 6. As shown in Figs. 7 and 8, the agreement between approximate and finite difference results for the shape factor H is excellent while agreement for momentum area $\bar{\theta}$, seen in Figs. 9 and 10, is good with a maximum difference

of 2.2 percent occurring at $x = 0.63$ for $Re = 10^6$. The finite difference results for the boundary-layer path, log (Re_s^*) versus H, closely follow the critical Reynolds number curve, although slightly above it. As is to be expected, increasing the Reynolds number moves the point of initial suction application forward, from $x = 0.495$ at $Re = 10^6$ to $x = 0.045$ at $Re = 10^7$. This dramatic shift is a consequence of the streamlined nose shape and favorable pressure gradient induced by the tunnel blockage.

The NSRDC body geometry is shown in Fig. 15, its pressure distribution in Fig. 16 and numerical results in Figs. 17 through 24. The streamlined nose, which fairs into a cylindrical midsection, causes a mild adverse pressure gradient to exist in the juncture region. Again the agreement in H at both Reynolds numbers is good except for the $Re = 10^6$ case for $x > 0.58$ where suction is not needed. In this region the approximate theory predicts a sudden dip in H which is less pronounced in the finite difference result. The maximum difference in H between the two in this region is 4.3 percent. When the $Re = 10^6$ solution was first run, the critical Reynolds number constraint was followed for $x > 0.58$ which resulted in blowing rather than suction in this region. A test was then put into the code to prevent blowing. Once the blowing was turned off for $x > 0.58$, the H distribution was found to undergo the sudden drop shown in Fig. 17. The comparison in Fig. 17 thus indicates that when the boundary layer undergoes a sudden change the approximate theory performs poorly at first but soon recovers. A further observation about the behavior of the H distribution, as shown in Figs. 17 and 18, is that when suction begins H slowly diminishes as x increases. This behavior is a reflection of the character of the critical Reynolds number curve. The $\bar{\theta}$ comparisons for this case, Figs. 19 and 20, are uniformly excellent and the finite difference results for the boundary-layer path, in

Figs. 21 and 22, are seen to follow the critical Reynolds number curve reasonably well, although slightly above it as in Case 1. The "choppiness" of the finite difference results is attributed to a numerically noisy pressure distribution. Finally, the peaks in the suction velocity distributions, in Figs. 23 and 24, correspond to the location of the maximum adverse pressure gradient which occurs at an x of about 0.175.

For the flat nose body, the geometry appears in Fig. 25 and the pressure distribution in Fig. 26. The numerical results for this case are shown in Figs. 27 through 38. The most significant feature of the pressure distribution is seen to be the very strong adverse pressure gradient present in the juncture region between the curved part of the nose and the cylindrical mid section. Figures 27 through 29 show the agreement for H to be good at all Reynolds numbers except in two regions on the body. The first is at $x \sim 0.03$ corresponding to where $\beta > 2$ in the finite difference solution. As already explained, β in the approximate solution cannot exceed 2, so that in such a region it is held constant at 2. Fortunately, the extent in arc length over which this occurs is very small ($\Delta x \sim 0.02$) so that the effect on the solution downstream is negligible. The second region of disagreement is in the vicinity of the maximum adverse pressure gradient, at $x \sim 0.1$. In the suction velocity distributions, shown in Figs. 36 through 38, the approximate theory predicts too high a suction peak in response to the maximum adverse pressure gradient. This high suction peak then forces H in the finite difference solution to dip below the approximate solution - see Figs. 27 through 29. The maximum difference in H between the two is 5.7% for $Re = 10^6$. In spite of the departure of H in the two solutions, the agreement for $\bar{\theta}$ is excellent at all Reynolds numbers, as shown in Figs. 30 through 32.

Finally, the boundary-layer path, Figs. 33 through 35, clearly indicates that the suction peak at $x \sim 0.1$, from the approximate theory, is too high, because the finite difference results suffer an excursion on the stable side of the critical Reynolds number curve. Afterward they follow the critical Reynolds number curve reasonably well, although slightly on the high side.

The final case is the F-57 low drag body extensively studied by Patel and Lee [6]. The Reynolds number of 1.2×10^6 corresponds to the value in their experiments. The body geometry is shown in Fig. 39 and the pressure distribution in Fig. 40. Patel and Lee point out that transition on this body occurs as a result of laminar separation followed by turbulent reattachment, in the vicinity of $x \sim 0.495$. As seen in Fig. 41, the approximate theory predicts a rapid rise in H downstream of the maximum body diameter, in response to the adverse pressure gradient. Once suction begins, at $x = 0.46$ (slightly upstream of maximum diameter) H begins to decrease with increasing x as a result of following the critical Reynols number curve. On the other hand, H from the finite difference solution of $x > 0.45$ rises at a slower rate but finally coincides again with the approximate solution at $x \sim 0.6$. As in the flat nose case, the approximate theory does not perform well in a region where the pressure gradient changes rapidly from favorable to adverse. The $\bar{\theta}$ distributions, nevertheless, agree extremely well, as Fig. 42 shows. The boundary-layer path, seen in Fig. 43, reflects the behavior seen in Fig. 41. The point where suction begins in the finite difference results is well below the critical Reynolds number curve (in the stable region). This means that the approximate theory predicts too much suction initially. The initial rise in suction speed in Fig. 44 is thus too rapid. The reason why

this solution was not run any further rearward on the body than x = 0.66 was that f_w at that point had nearly exceeded the limit of the data base (2.5).

4. CONCLUSIONS

The extension of Smith's piecewise similarity method to the prediction of the minimum distributed suction required to maintain laminar flow in an axisymmetric boundary layer provides an automated design tool that is both fast and reasonably accurate for a variety of body shapes and Reynolds numbers. In cases which possess pressure gradients that change rapidly from favorable to adverse, especially when the adverse pressure gradient is strong, the method overpredicts the suction speed in the vicinity of the maximum adverse pressure gradient. Thus, it errs on the side of conservatism.

The most sensitive (and most meaningful) measure of the accuracy of the approximate method is the boundary-layer path, log (Re_{δ^*}) versus H, as obtained from a finite-difference solution which uses the suction velocity distribution from the approximate theory. For the four bodies studied, the finite difference solution was found to follow the critical Reynolds number curve quite well indicating that the correct amount of suction was being predicted. As already indicated, any excursions of the finite-difference results from this curve were into the stable region. Finally, in all cases examined, the agreement between approximate and finite-difference results for the momentum area distribution, $\bar{\theta}$ versus x, was excellent.

REFERENCES

1. Rosenhead, L. (Editor), Laminar Boundary Layers, Oxford University Press, (1963).

2. Walz, A., "Ein neuer Ansatz für das Geschwindigkeitsprofil der Laminaren Reibungsschicht," Ber. Lilienthal-Ges. Luftfahrt., No. 141, pp. 8-12, (1941).

3. Smith, A. M. O., "Rapid Boundary-Layer Calculations by Piecewise Application of Similar Solutions," Journal Aeronautical Sciences, Vol. 23, pp. 901-912 (October 1956).

4. Wazzan, A. R., C. Gazley, Jr. and A. M. O. Smith, "H-R_x Method for Predicting Transition," AIAA Journal, Vol. 19, pp. 810-811 (June 1981).

5. Keller, H. B., "Accurate Difference Methods for Nonlinear Two-Point Boundary Value Problems," SIAM Journal Numerical Analysis, Vol. 11, pp. 305-320 (April 1974).

6. Patel, V. C. and Y. T. Lee, "Thick Axisymmetric Turbulent Boundary Layer and Near Wake of a Low-Drag Body of Revolution," Iowa Institute of Hydraulic Research Rept. IIHR No. 210, University of Iowa, Iowa City, Iowa (December 1977).

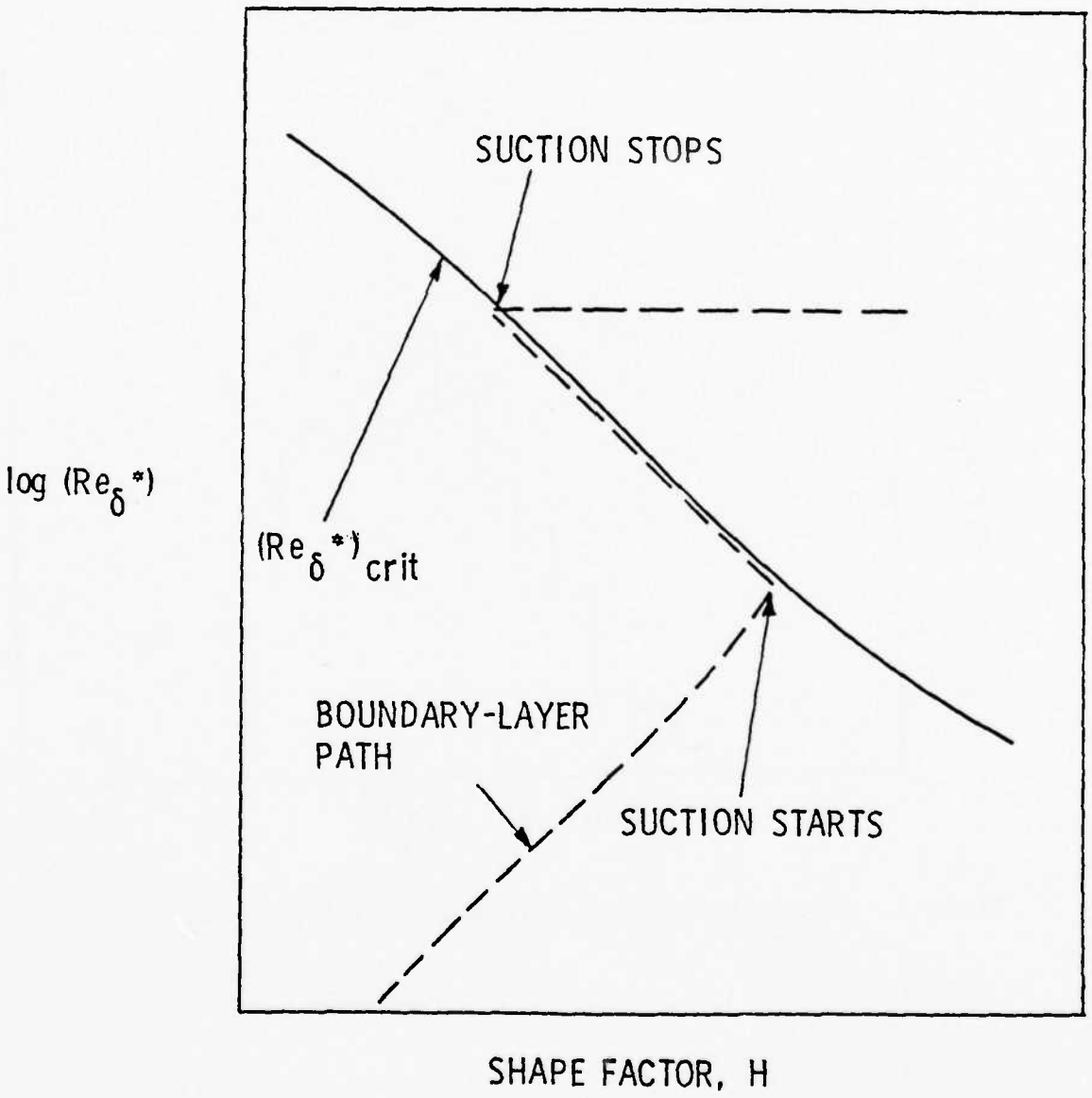

Figure 1. Schematic of Path of Boundary-Layer Development, log (Re$_{\delta}$*) vs. H.

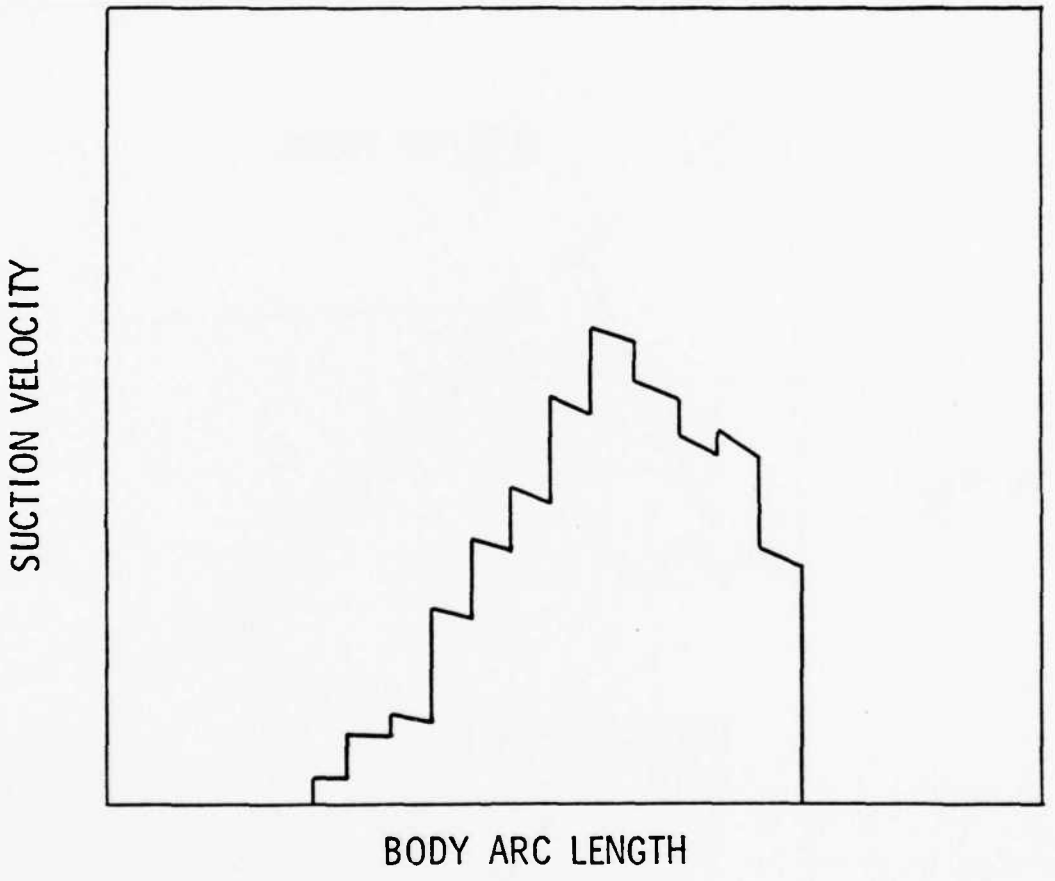

Figure 2. Schematic of Saw-Tooth Behavior of Suction Velocity.

--

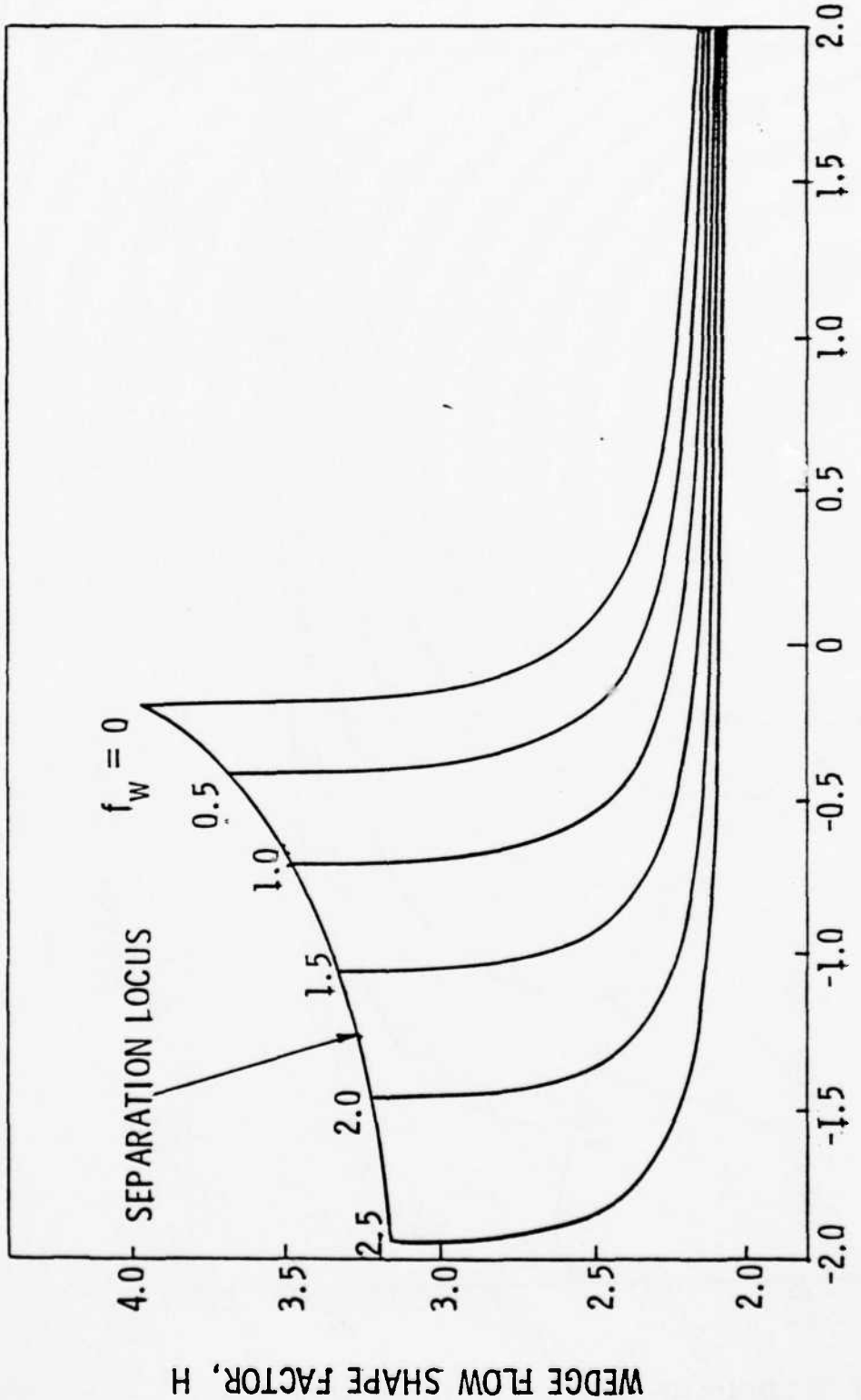

Figure 3. Wedge Flow Shape Factor from Falkner-Skan Equation.

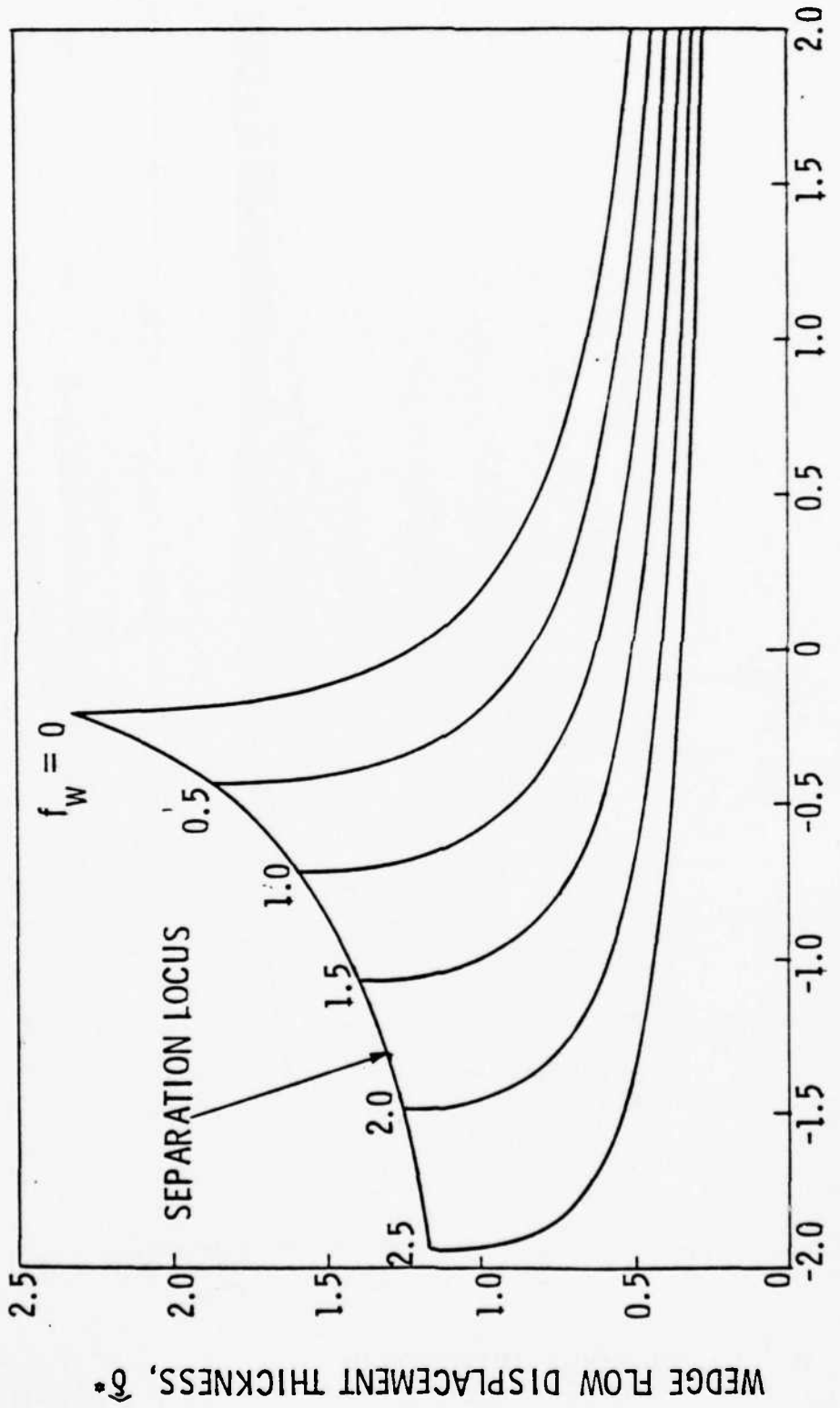

Figure 4. Wedge Flow Displacement Thickness from Falkner-Skan Equation.

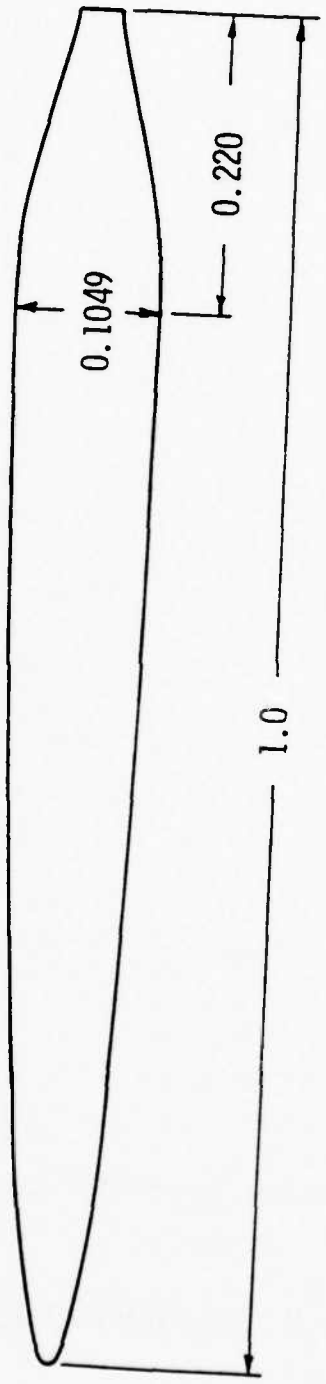

Figure 5. Laminar Flow Body Geometry.

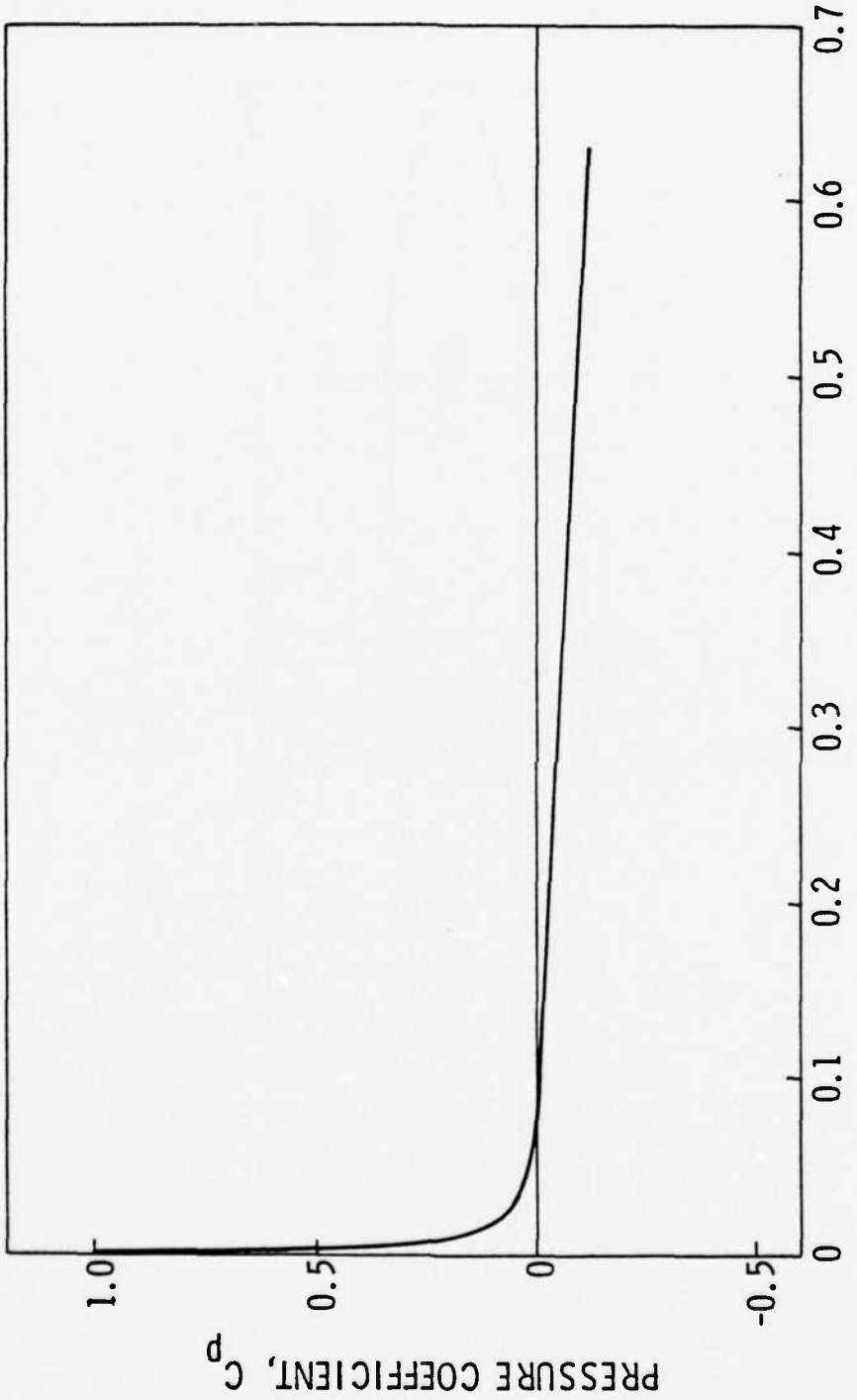

Figure 6. Pressure Distribution, Laminar Flow Body in Tunnel.

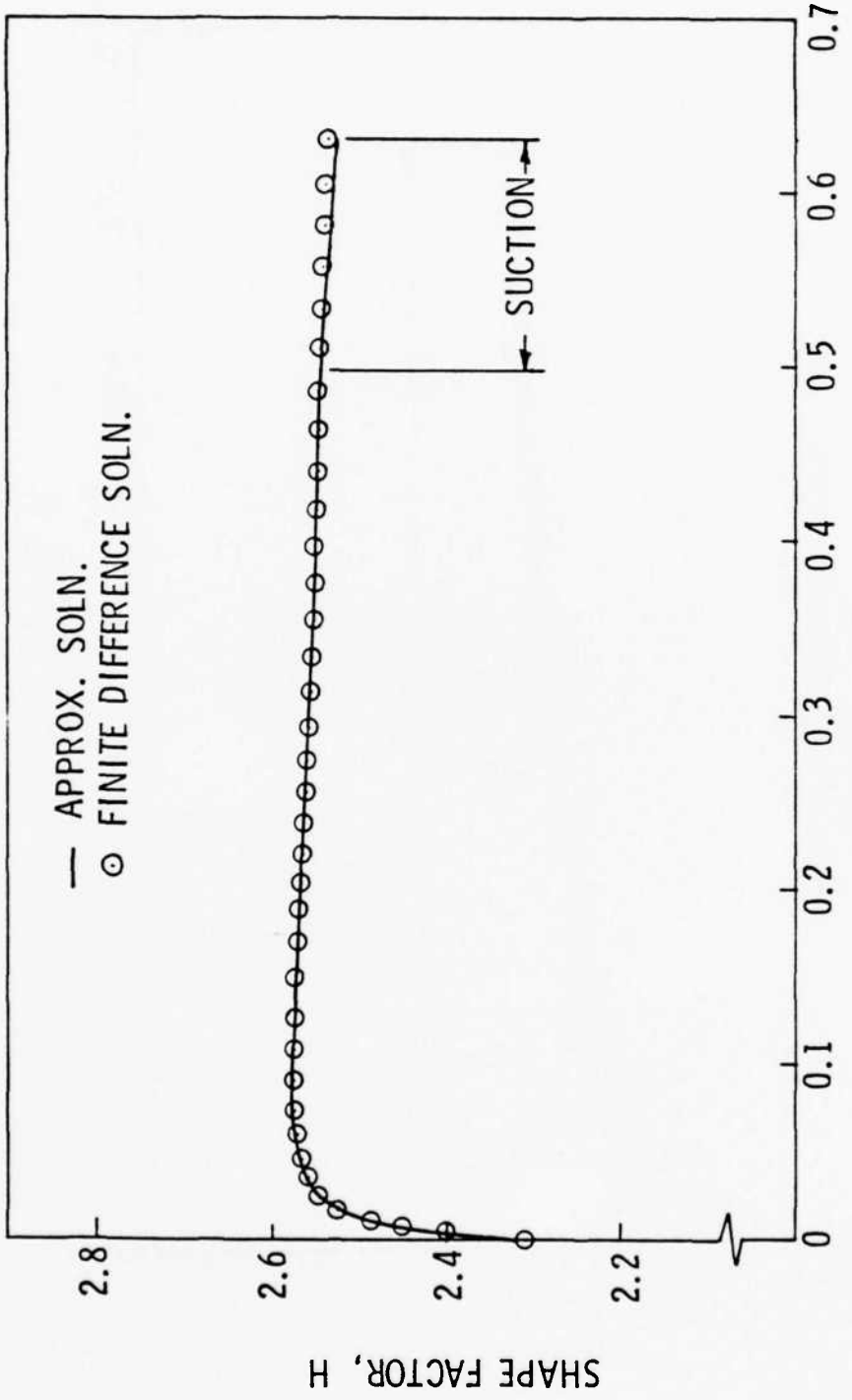

Figure 7. Boundary-Layer Shape Factor Distribution, Laminar Flow Body in Tunnel, Re = 10^6.

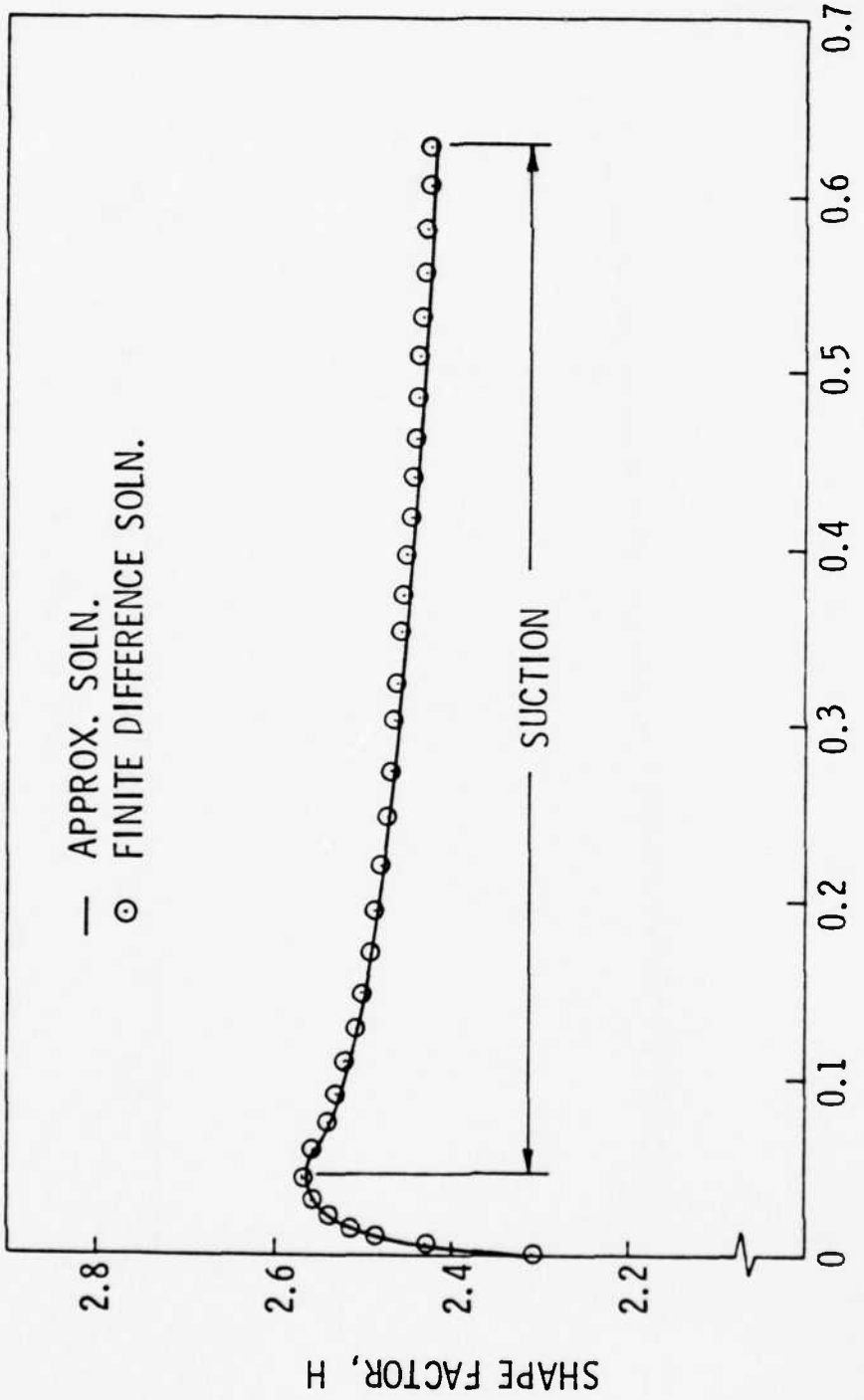

Figure 8. Boundary-Layer Shape Factor Distribution, Laminar Flow Body in Tunnel, $Re = 10^7$.

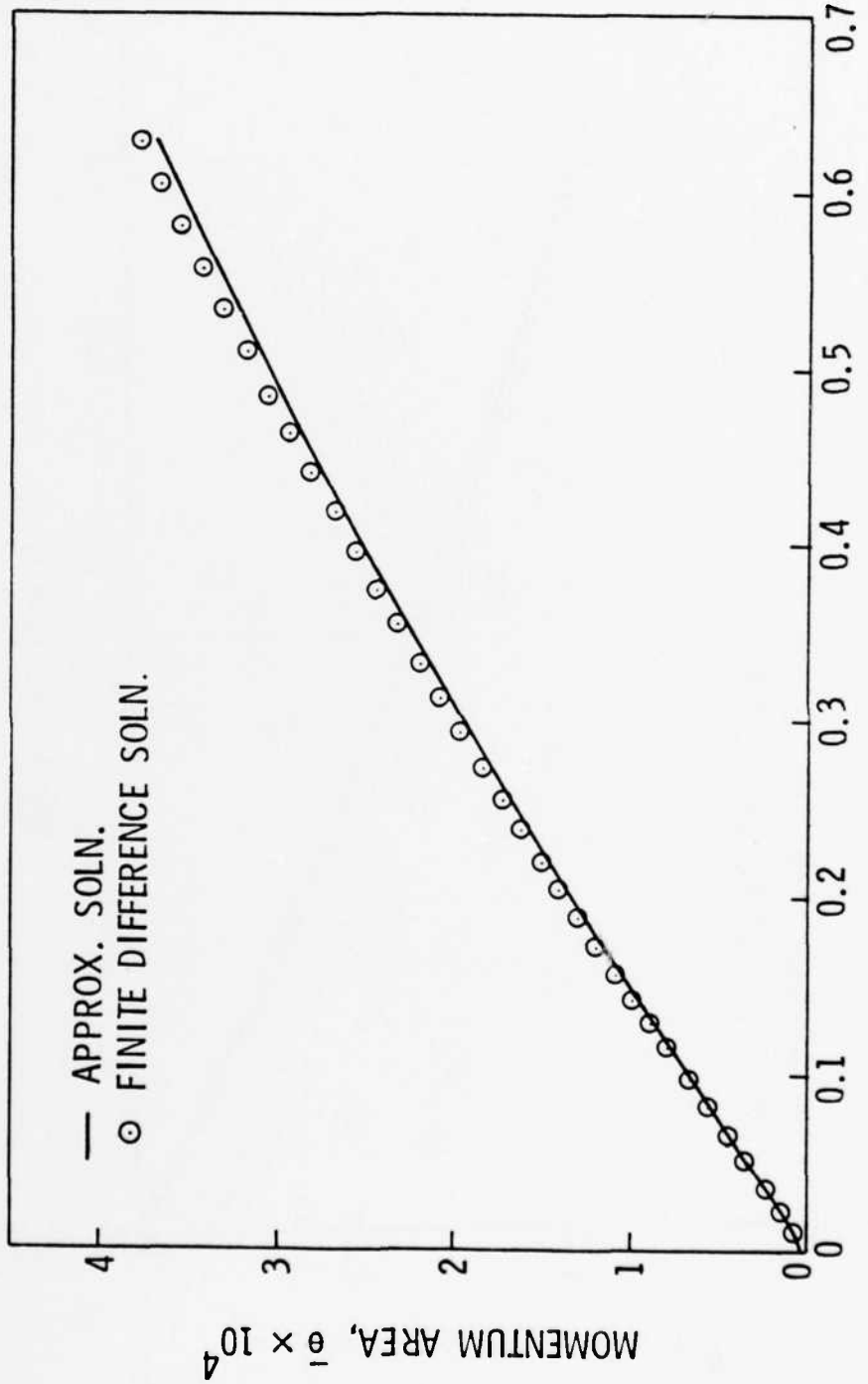

Figure 9. Boundary-Layer Momentum Area Distribution, Laminar Flow Body in Tunnel, Re = 10^6.

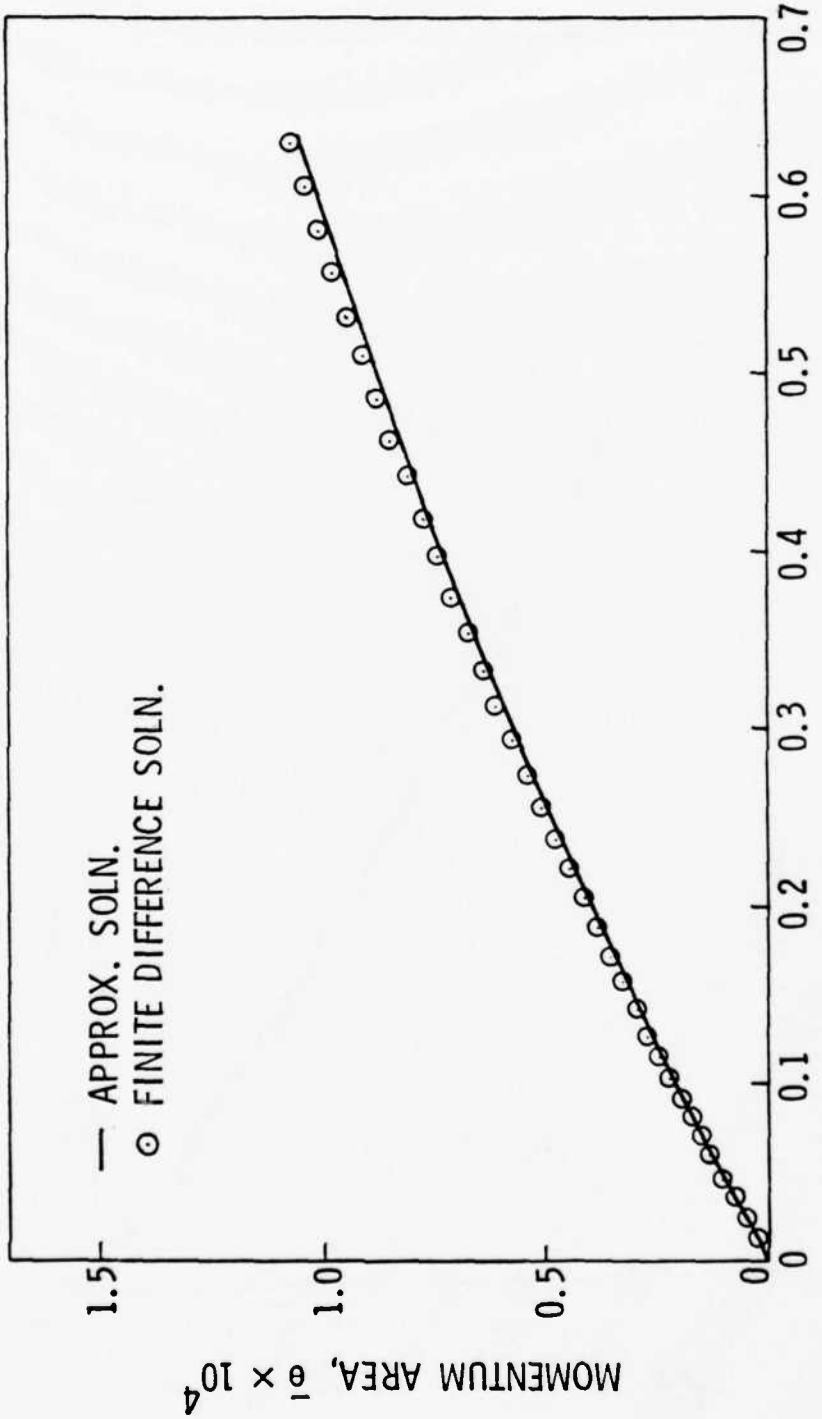

Figure 10. Boundary-Layer Momentum Area Distribution, Laminar Flow Body in Tunnel, Re = 10^7.

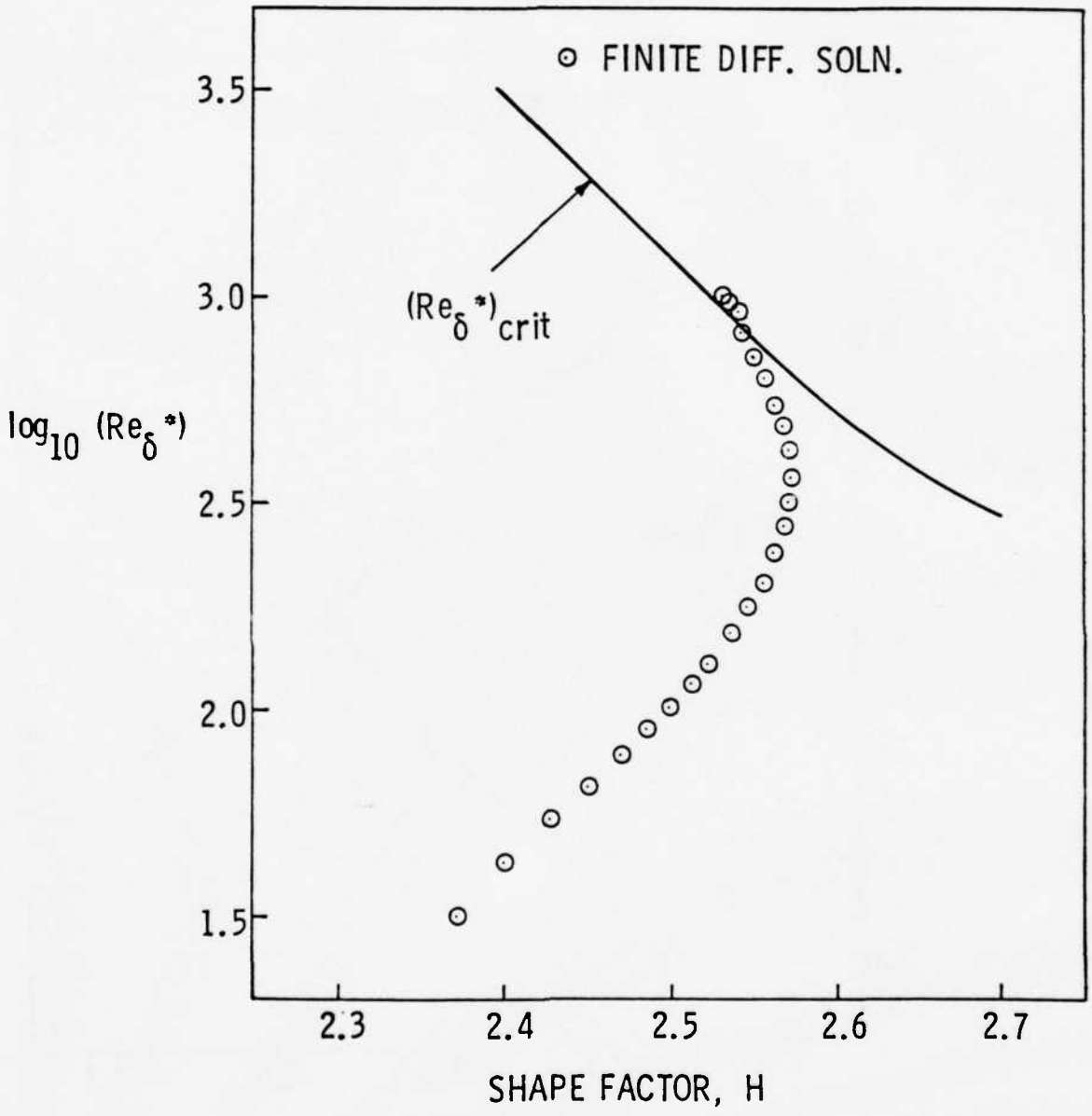

Figure 11. Path of Boundary-Layer Development, log ($Re_\delta{}^*$) vs. H, Laminar Flow Body in Tunnel, Re = 10^6.

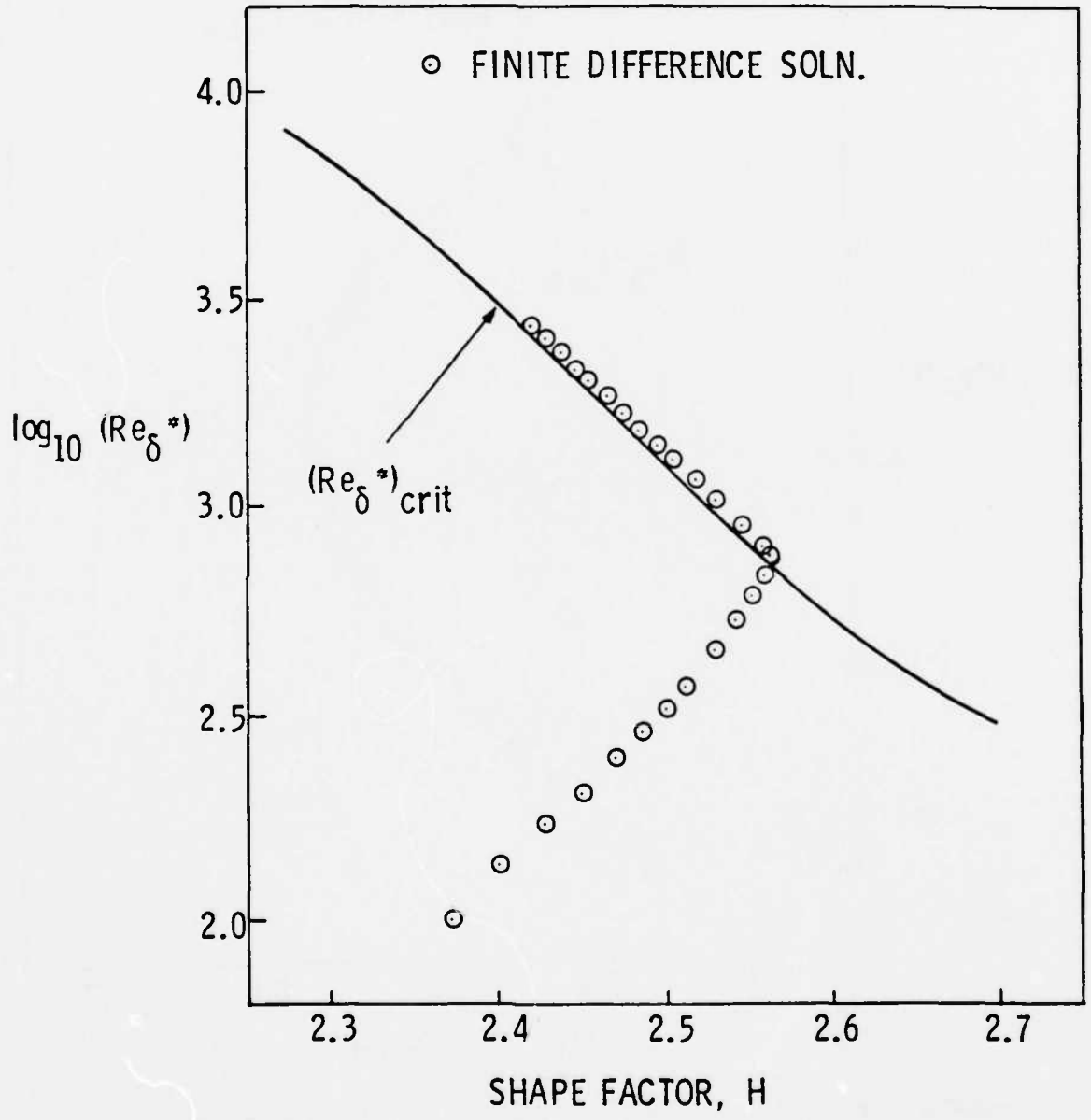

Figure 12. Path of Boundary-Layer Development, log ($Re_\delta{}^*$) vs. H, Laminar Flow Body in Tunnel, Re = 10^7.

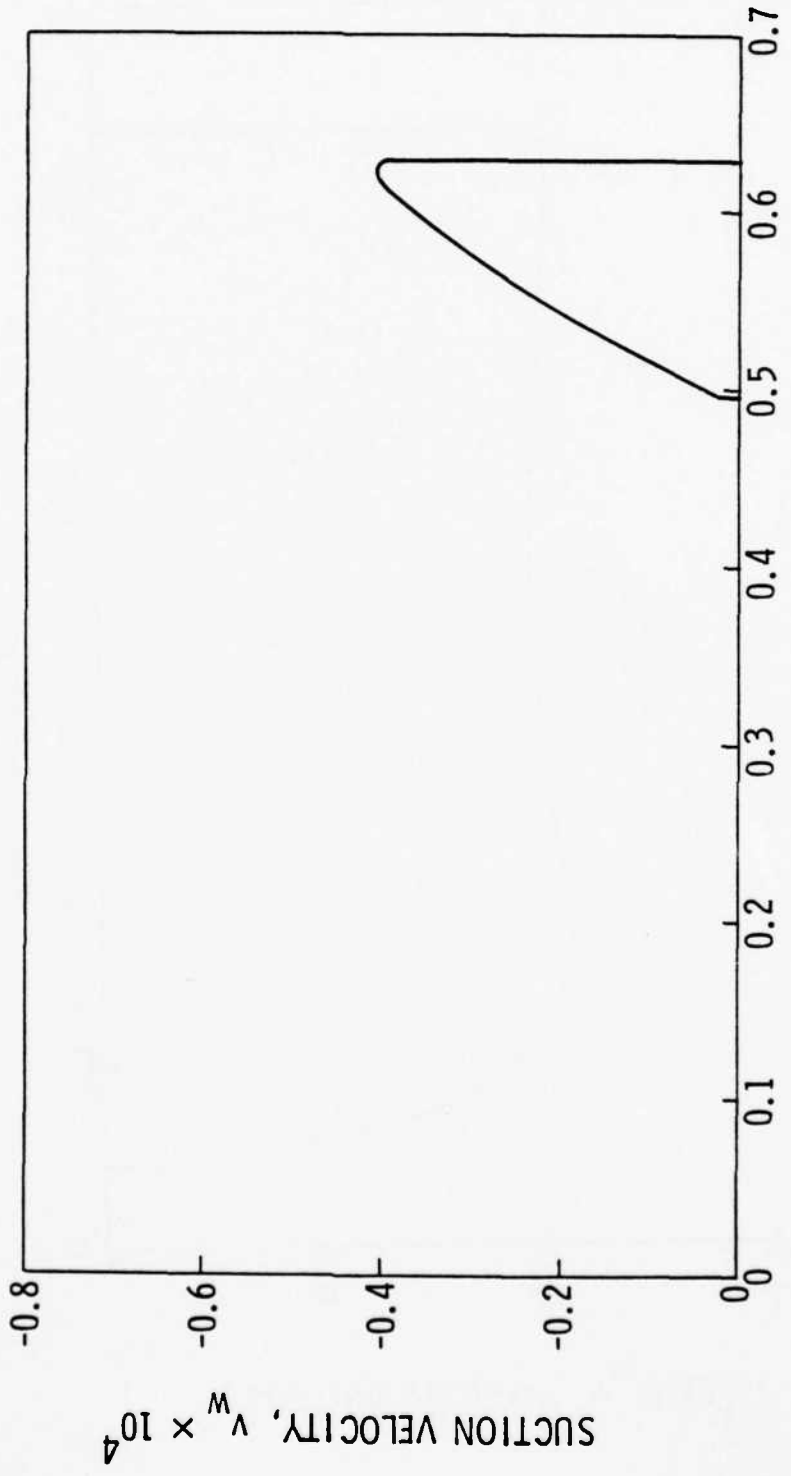

Figure 13. Suction Velocity Distribution, Laminar Flow Body in Tunnel, Re = 10^6.

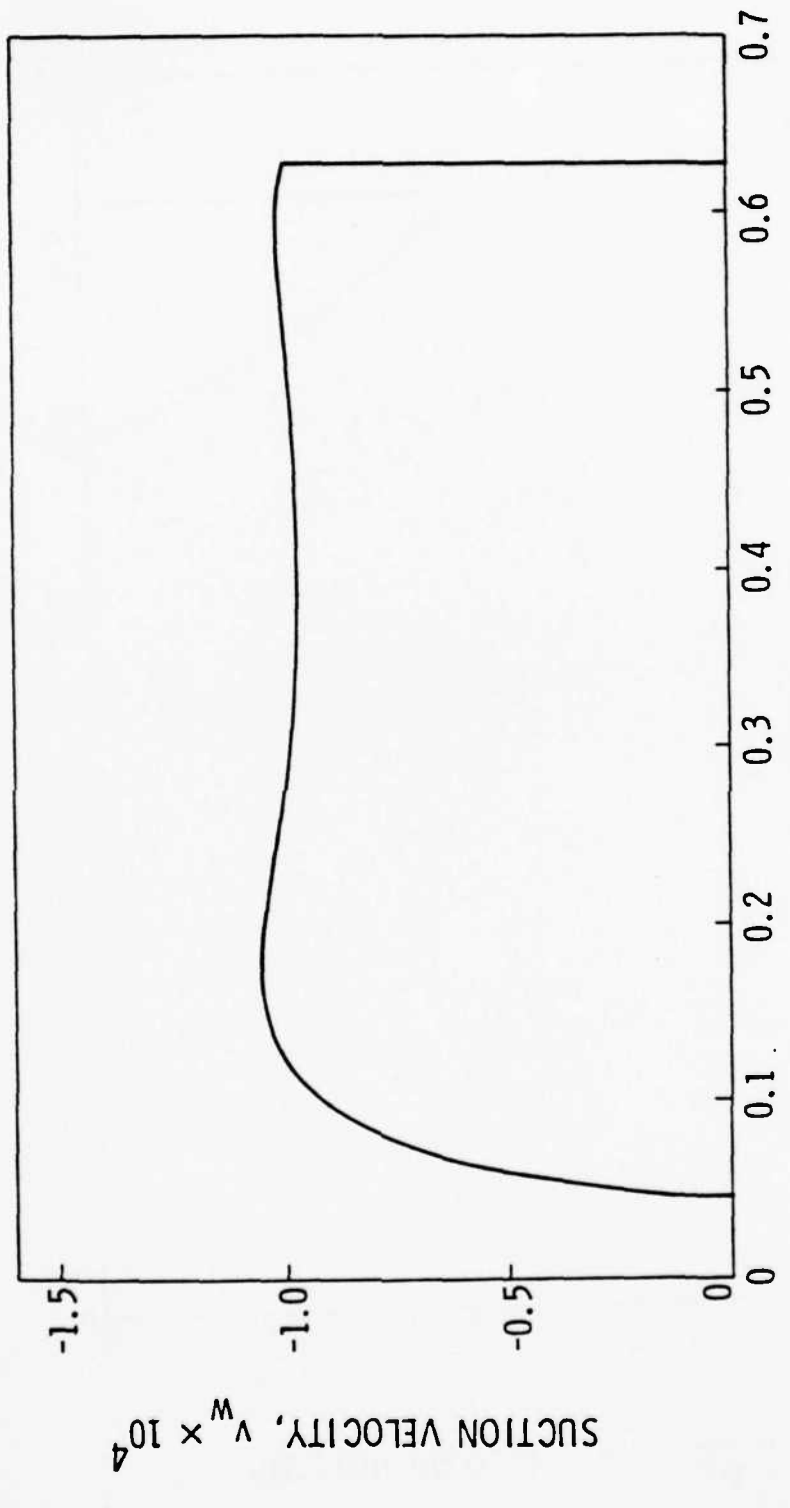

Figure 14. Suction Velocity Distribution, Laminar Flow Body in Tunnel, Re = 10^7.

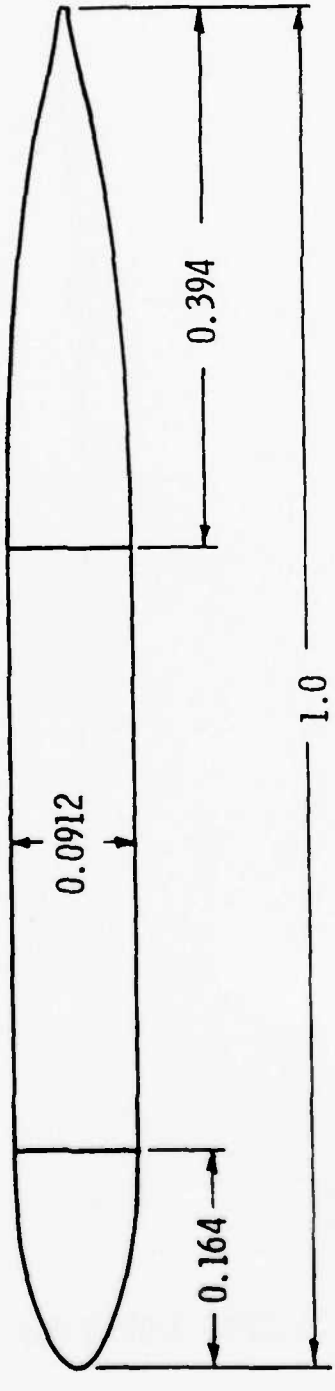

Figure 15. NSRDC Body Geometry.

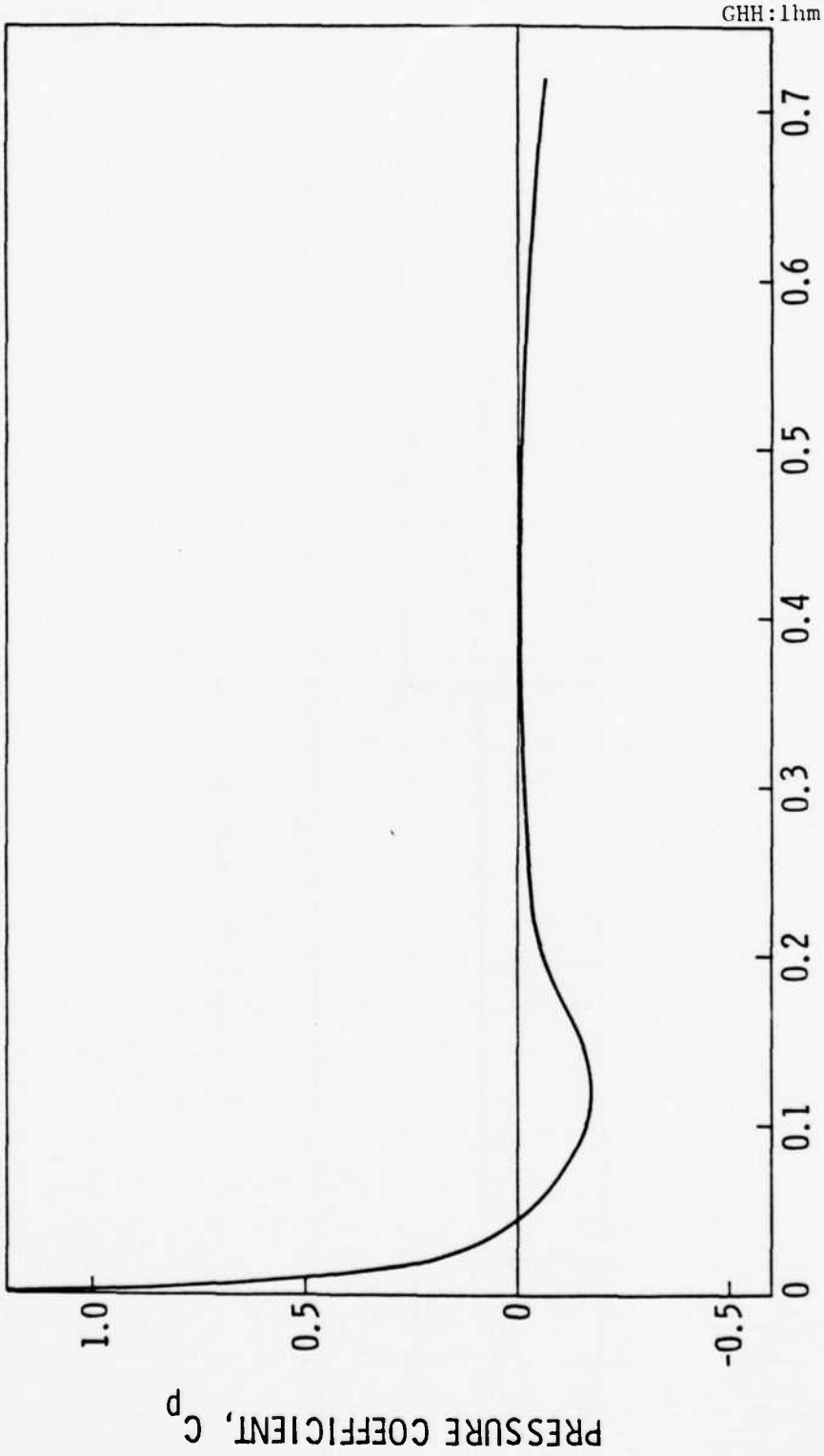

Figure 16. Pressure Distribution, NSRDC Body.

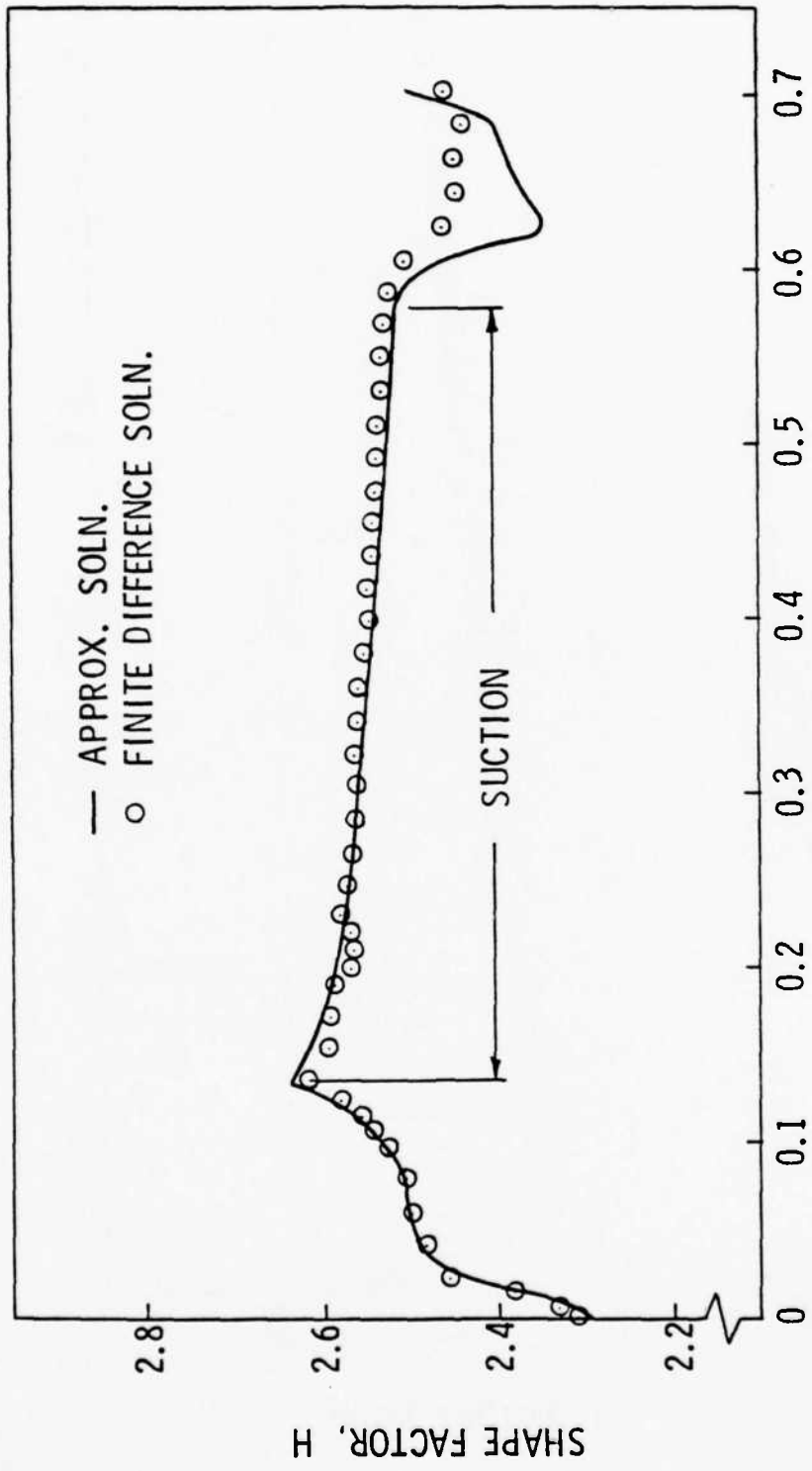

Figure 17. Boundary-Layer Shape Factor Distribution, NSRDC Body, Re = 10^6.

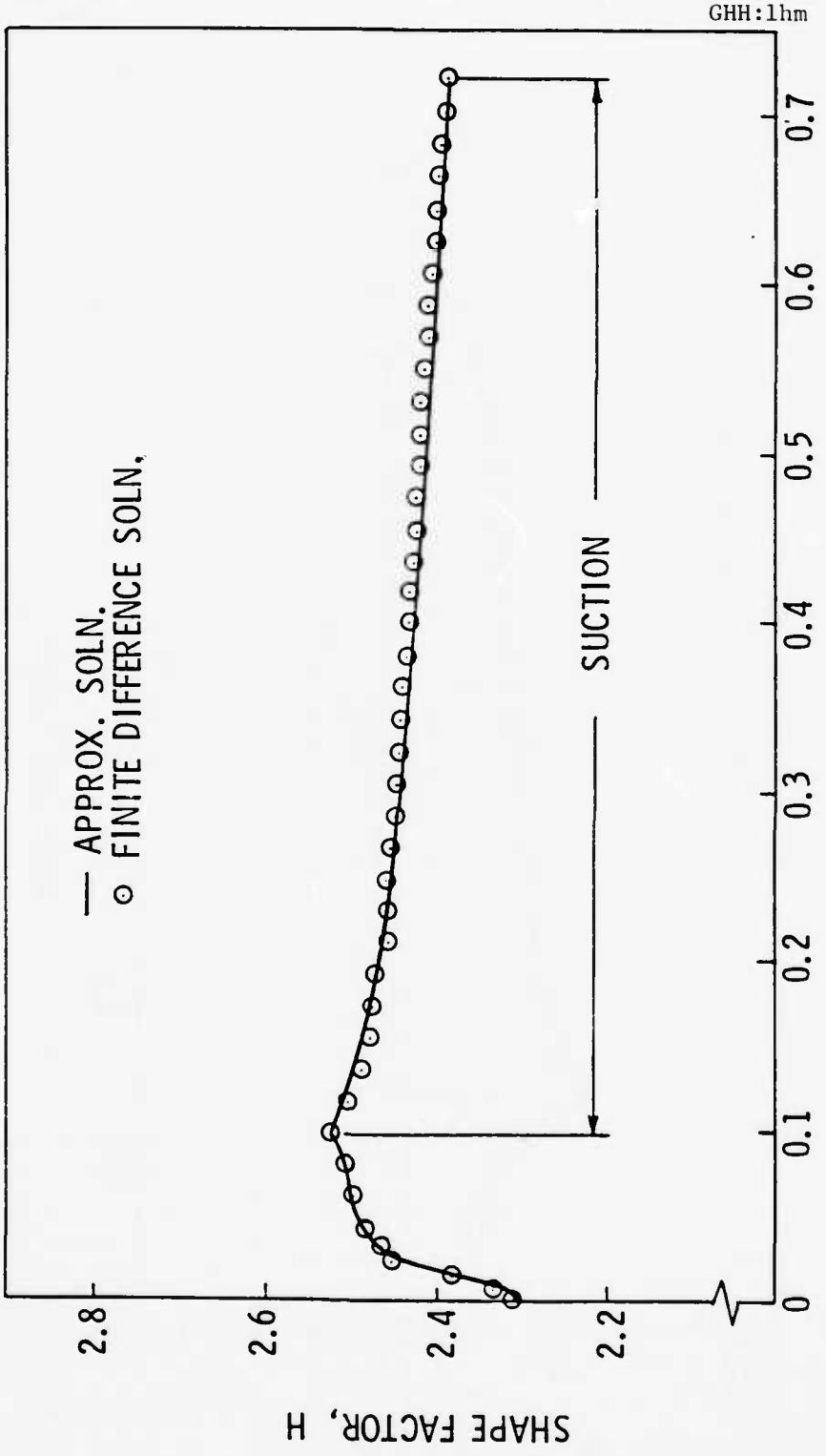

Figure 18. Boundary-Layer Shape Factor Distribution, NSRDC Body, $Re = 10^7$.

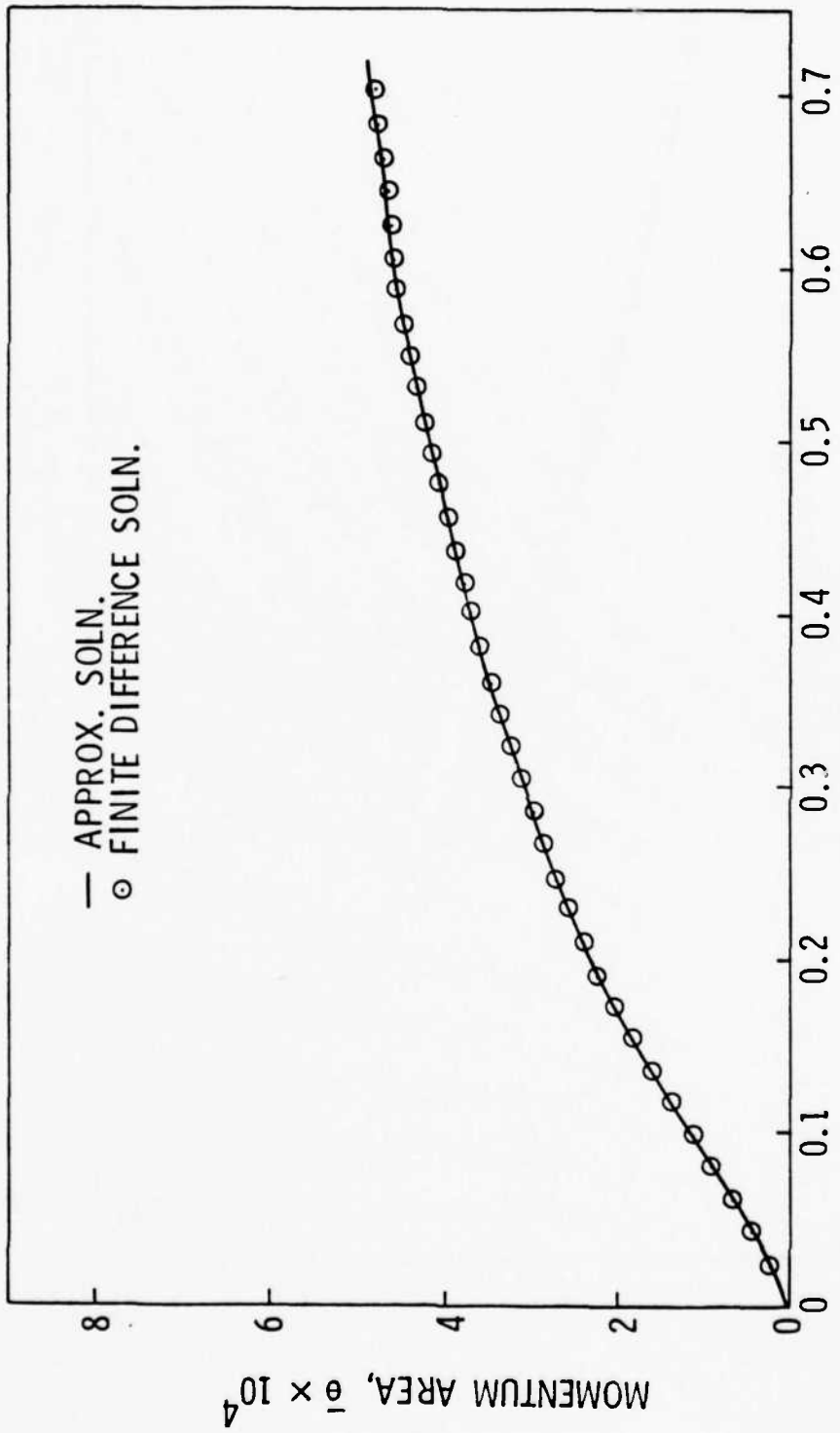

Figure 19. Boundary-Layer Momentum Area Distribution, NSRDC Body, Re = 10^6.

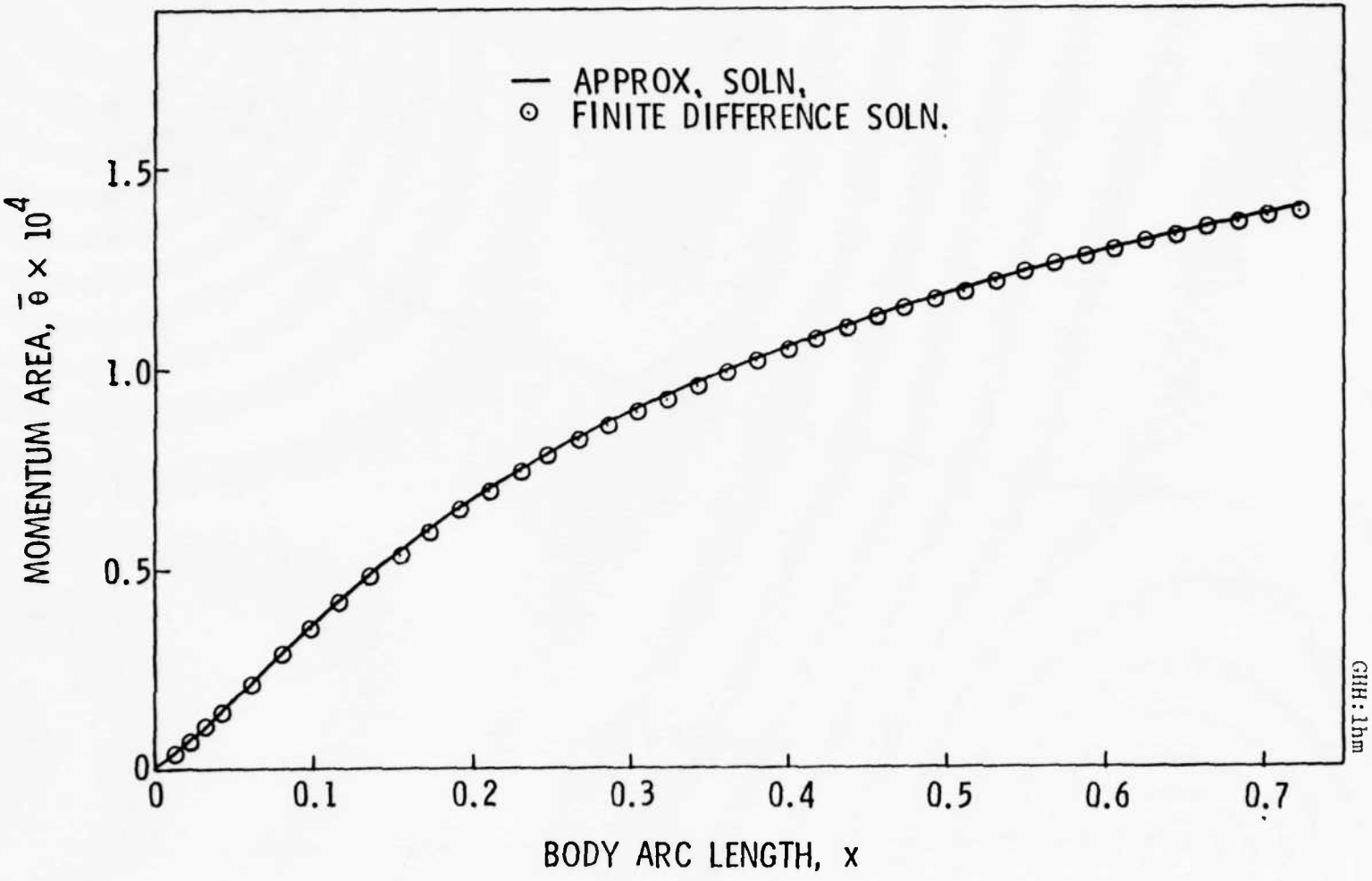

Figure 20. Boundary-Layer Momentum Area Distribution, NSRDC Body, Re = 10^7.

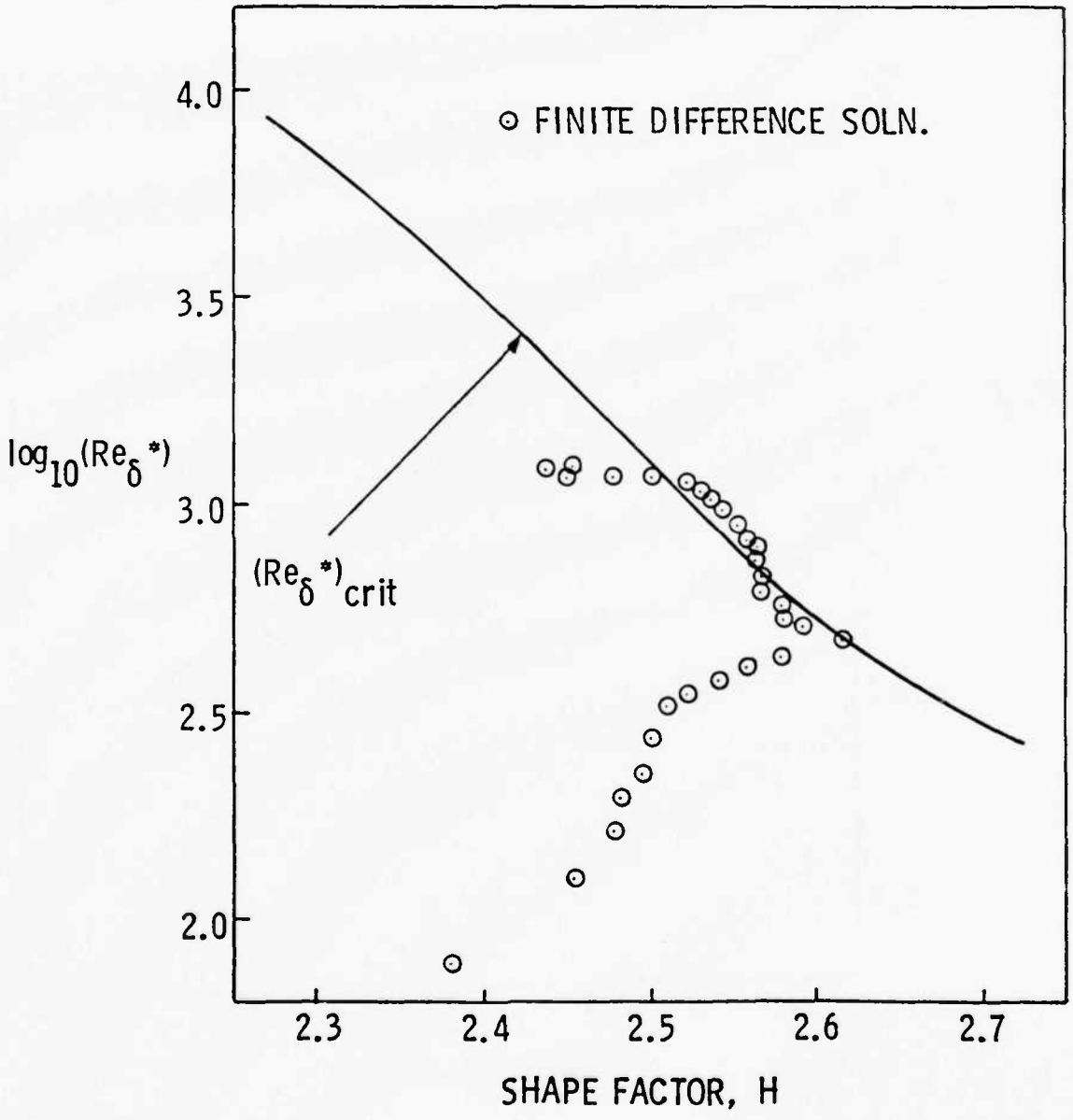

Figure 21. Path of Boundary-Layer Development, log ($Re_\delta{}^*$) vs. H, NSRDC Body, Re = 10^6.

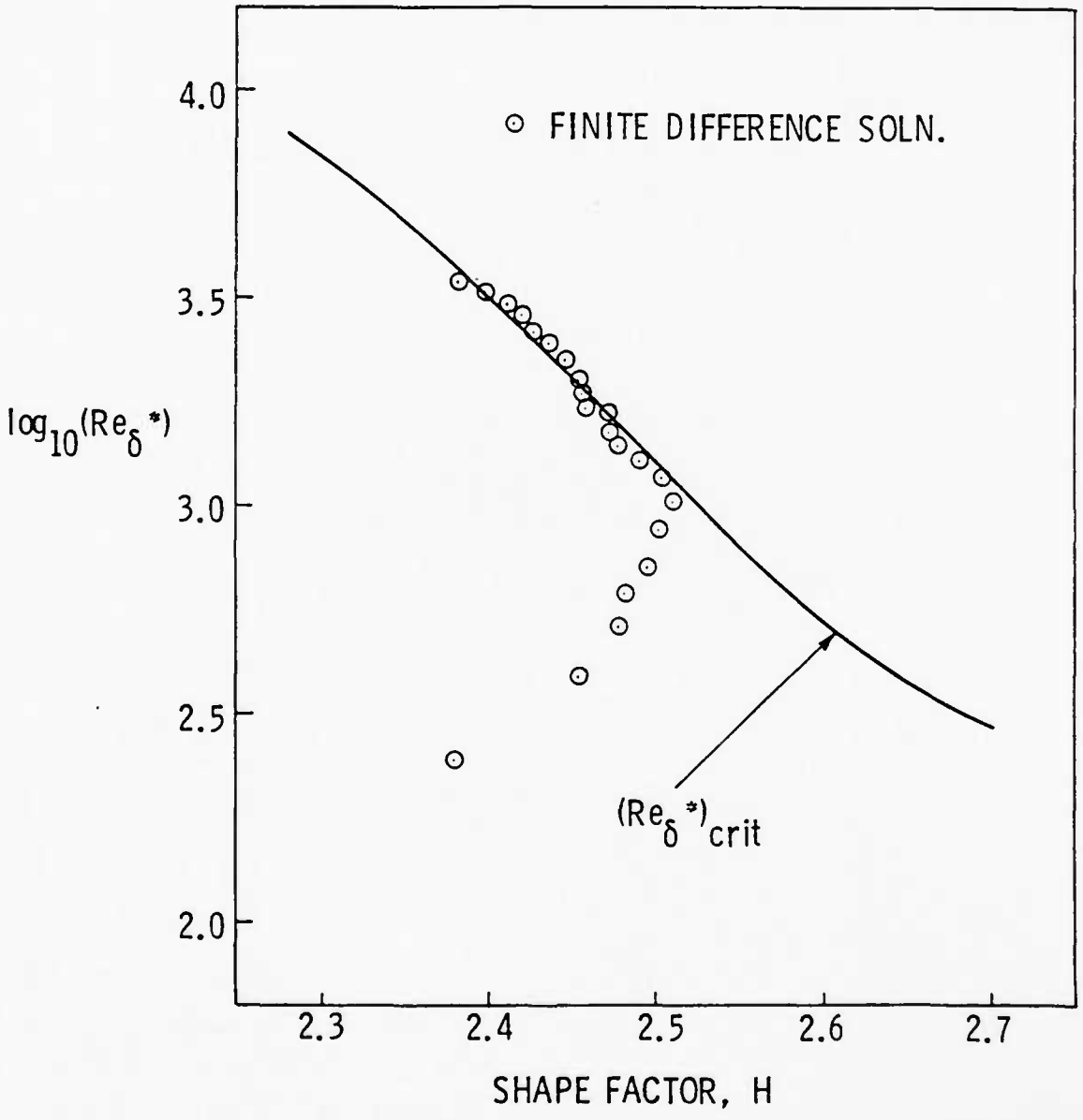

Figure 22. Path of Boundary-Layer Development, log ($Re_\delta{}^*$) vs. H, NSRDC Body, Re = 10^7.

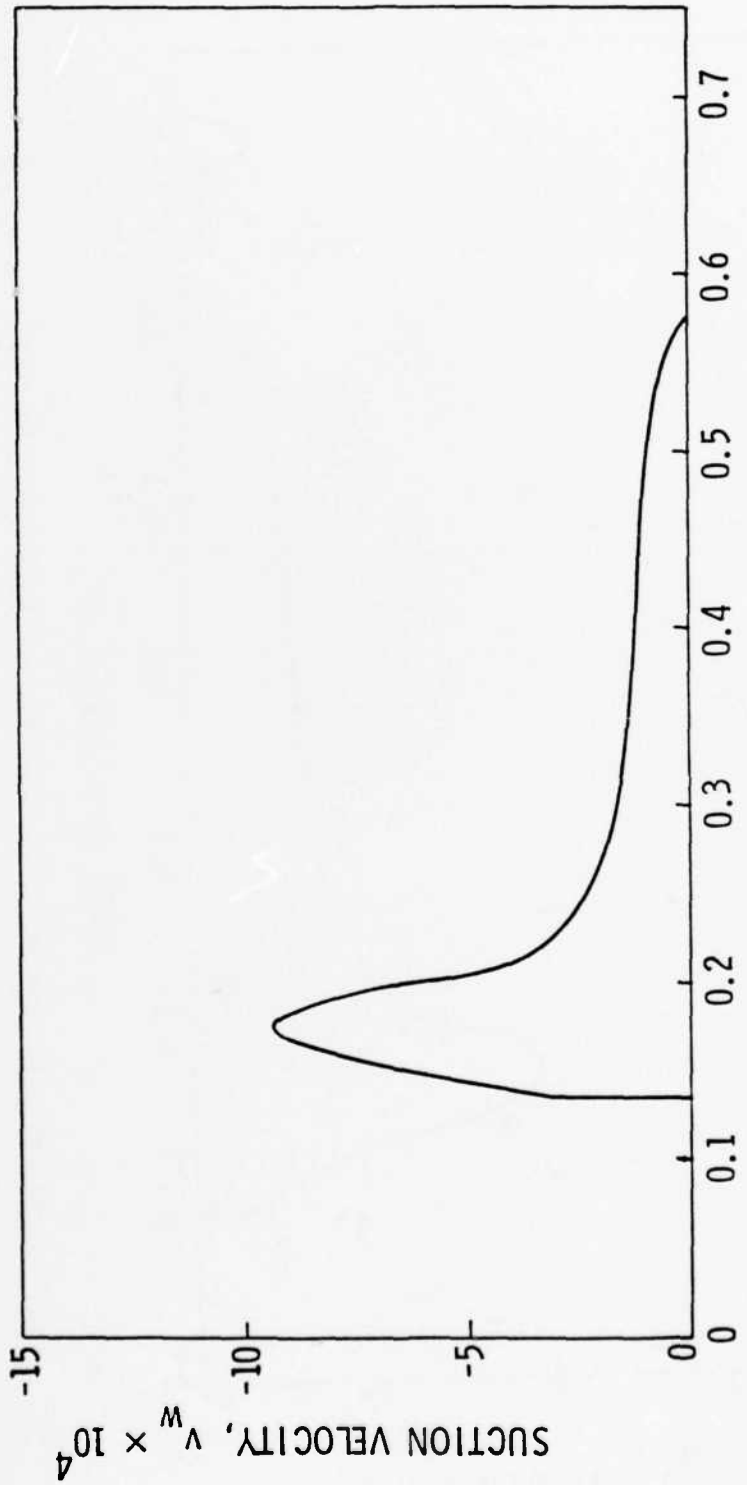

Figure 23. Suction Velocity Distribution, NSRDC Body, Re = 10^6.

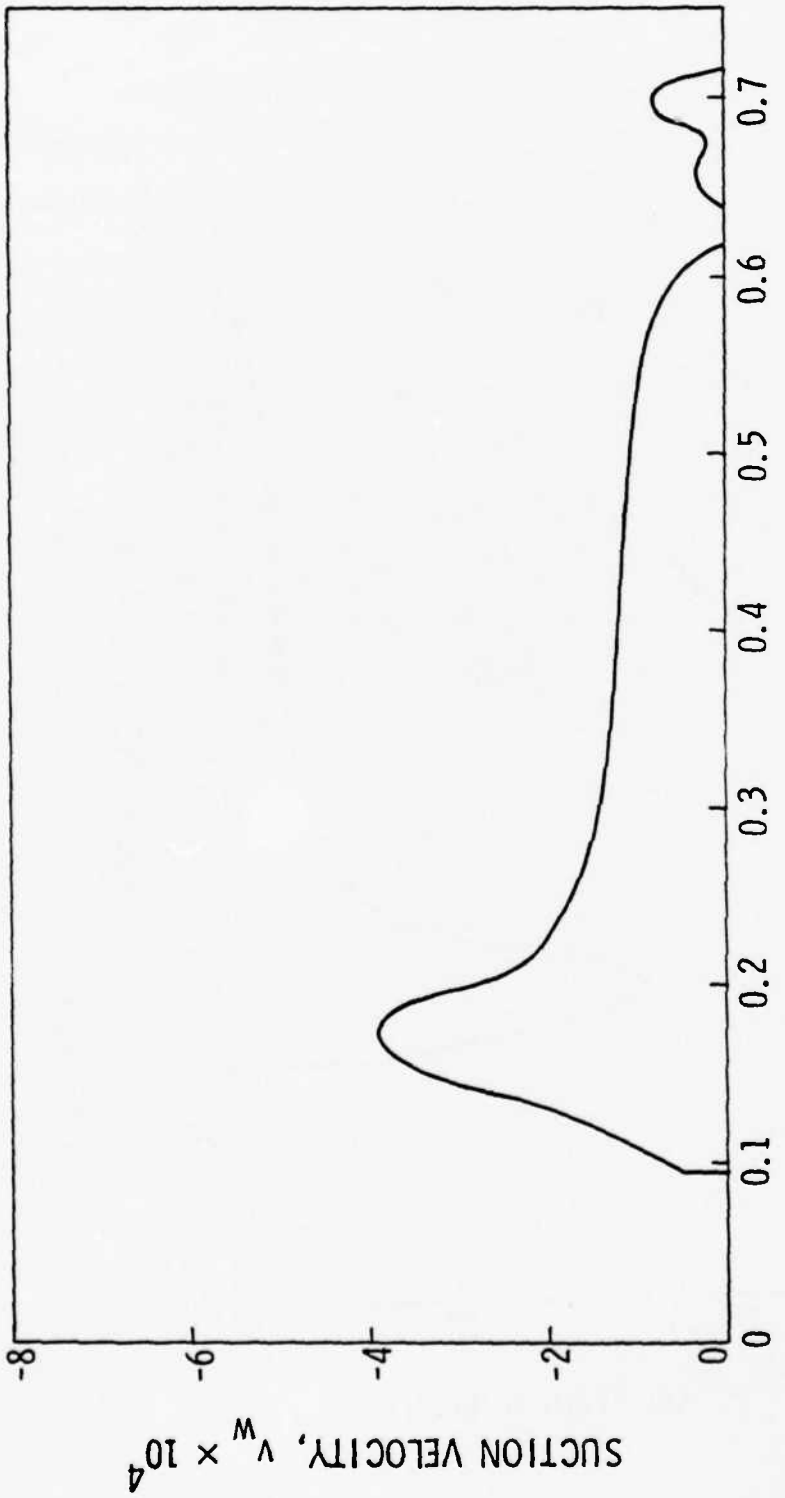

Figure 24. Suction Velocity Distribution, NSRDC Body, Re = 10^7.

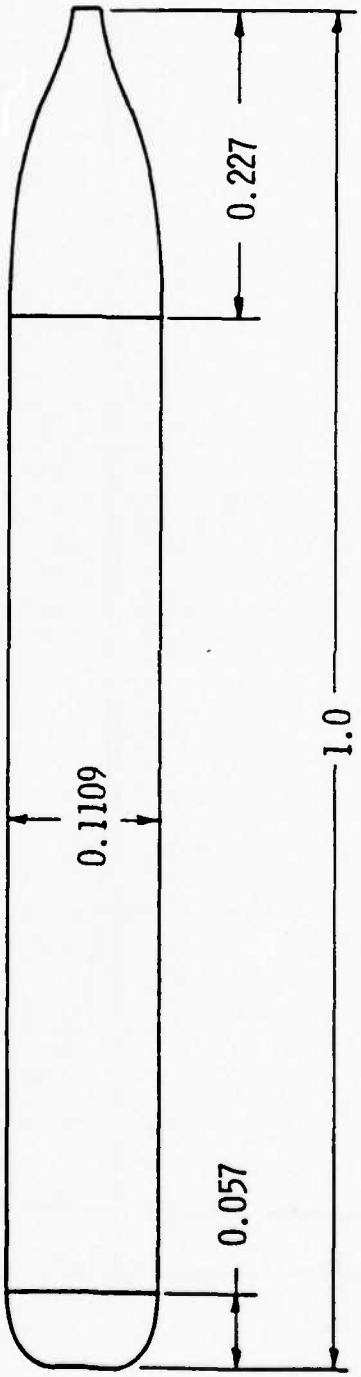

Figure 25. Flat Nose Body Geometry.

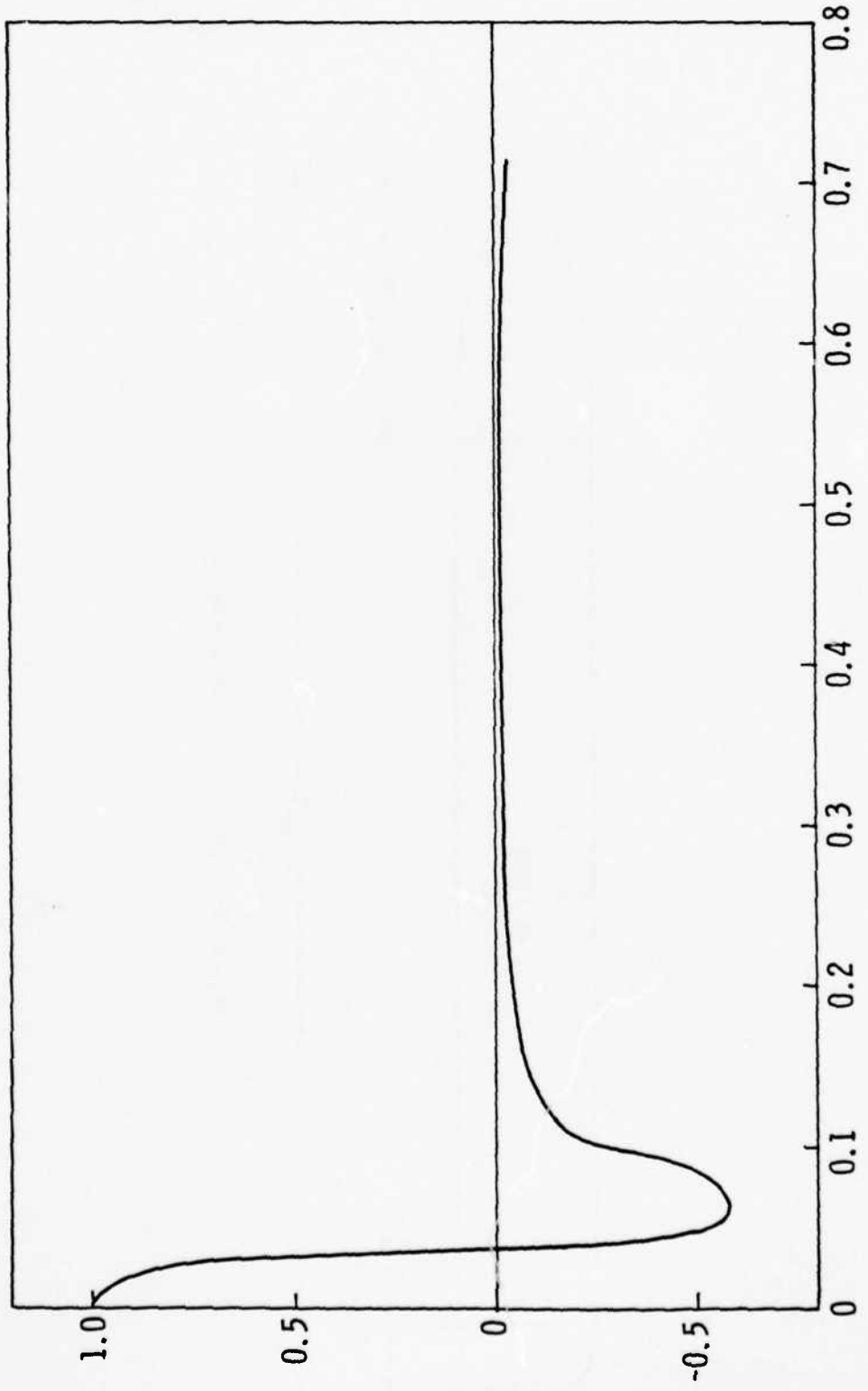

Figure 26. Pressure Distribution, Flat Nose Body.

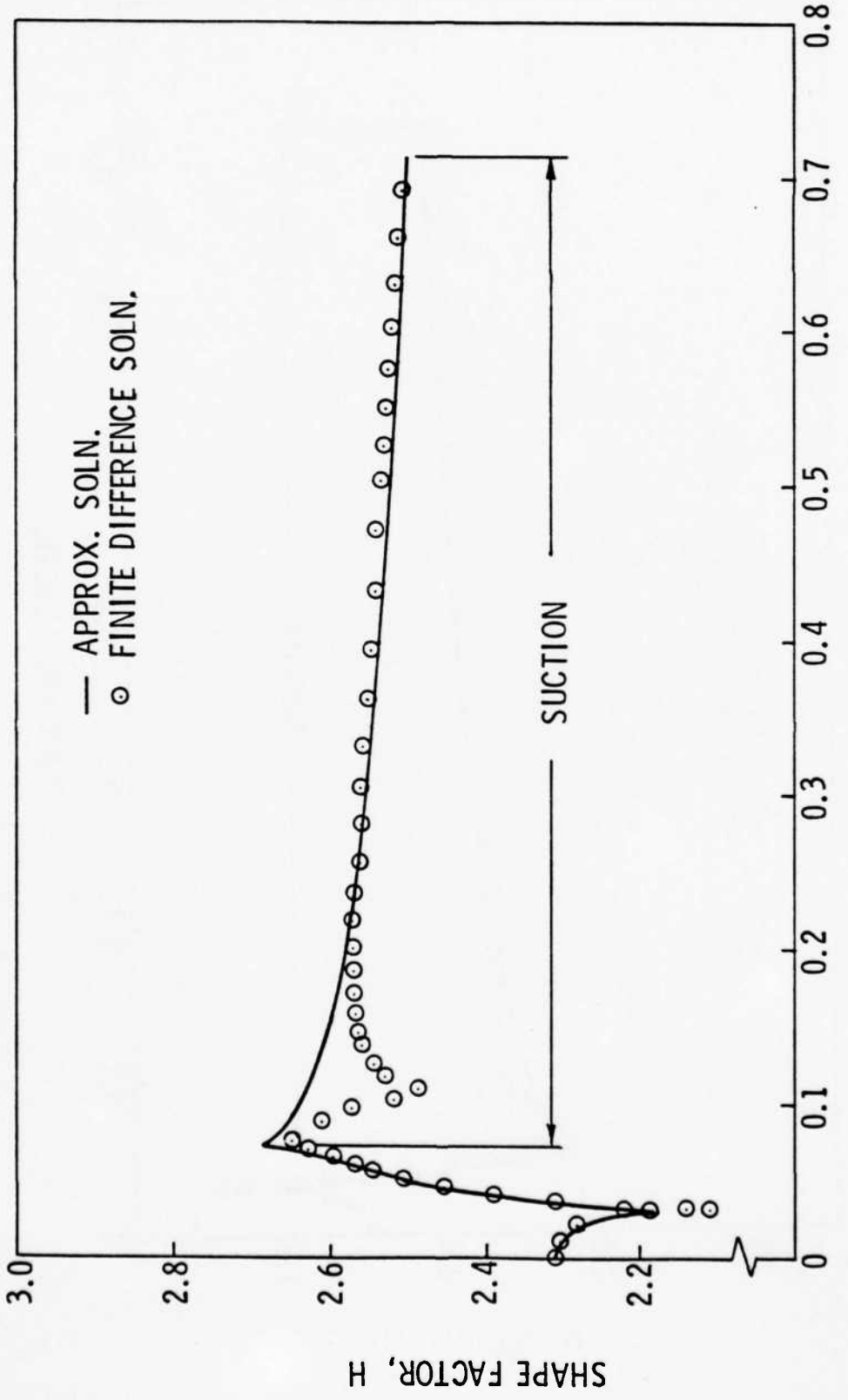

Figure 27. Boundary-Layer Shape Factor Distribution, Flat Nose Body, Re = 10^6.

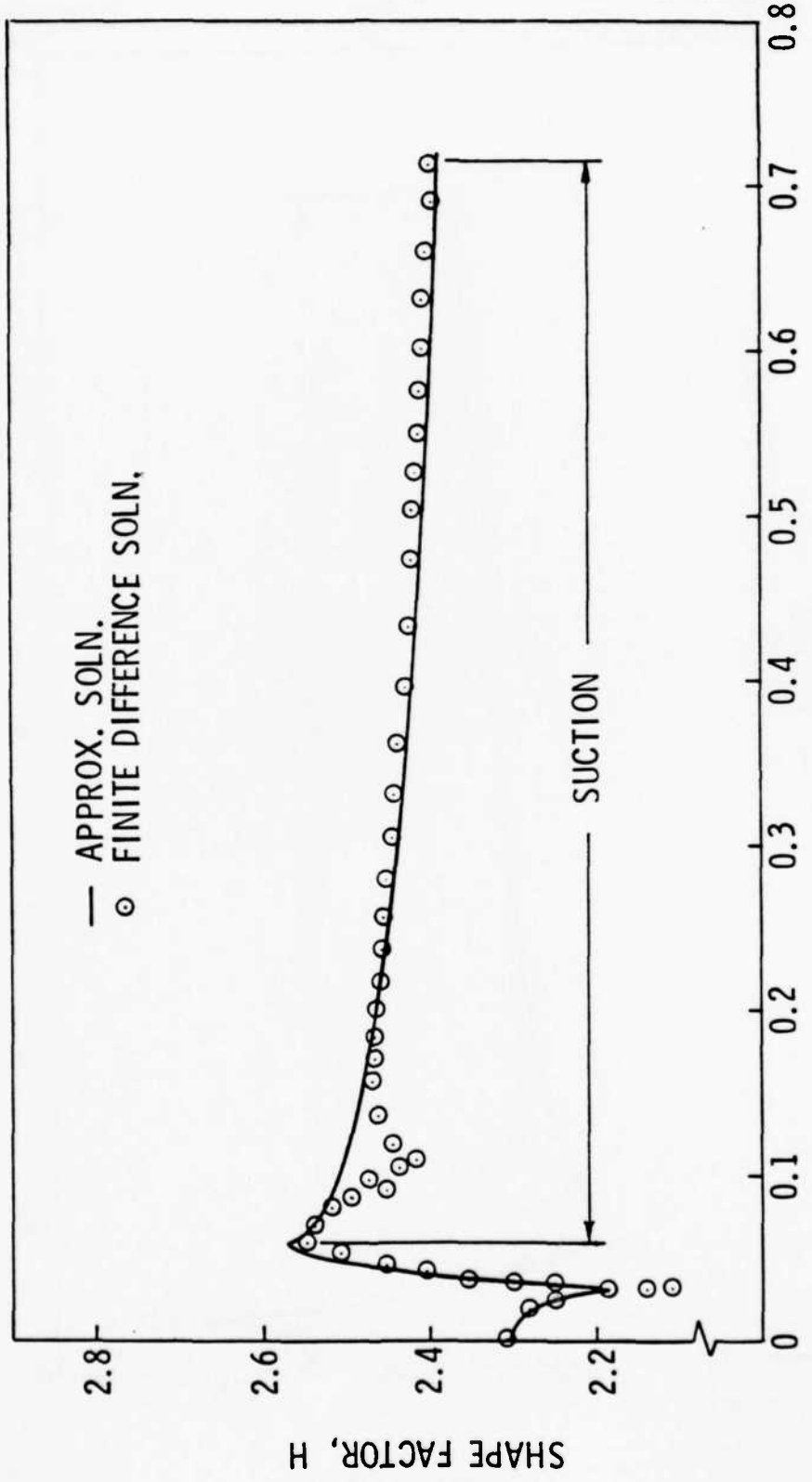

Figure 28. Boundary-Layer Shape Factor Distribution, Flat Nose Body, Re = 10^7.

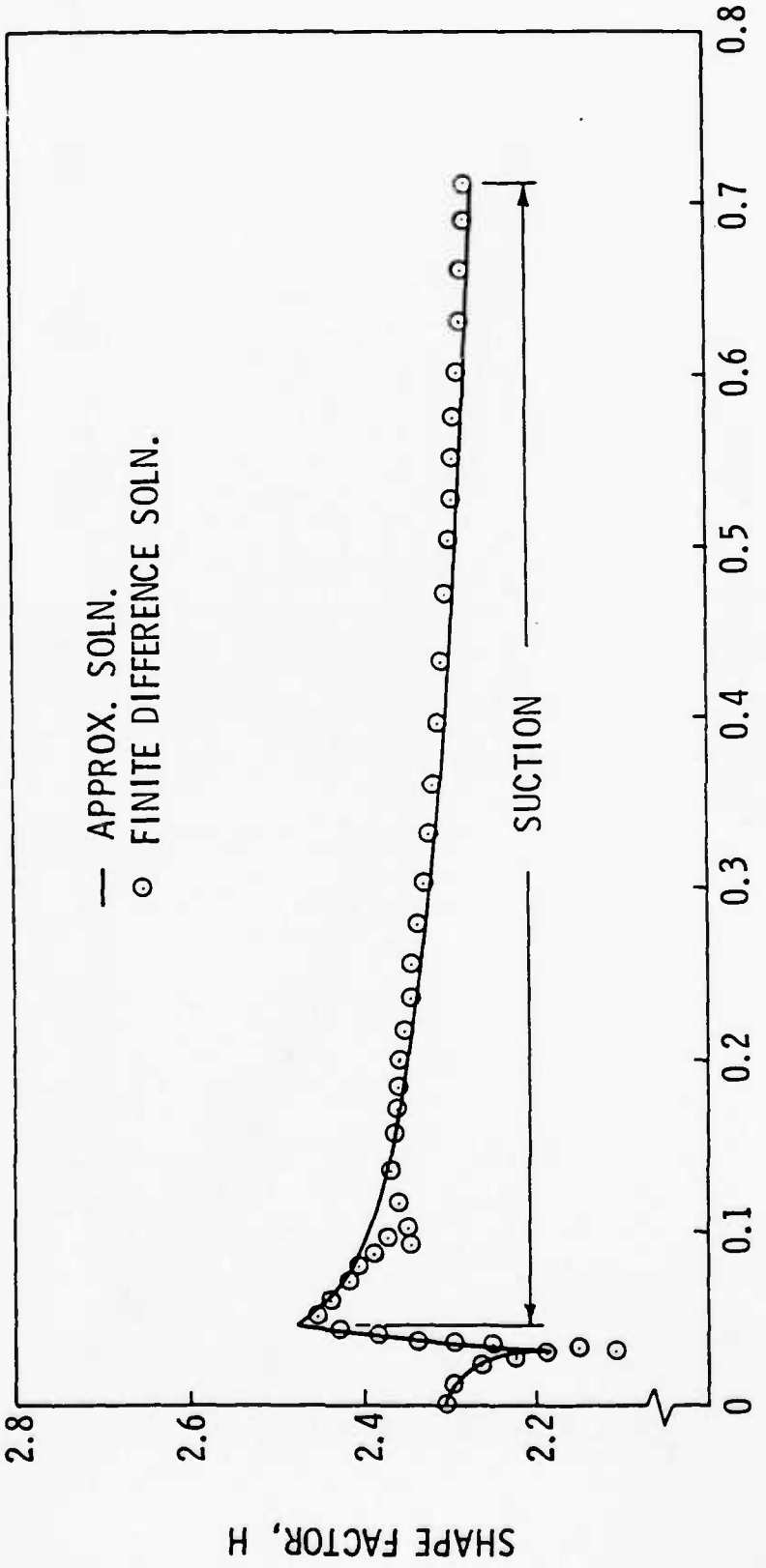

Figure 29. Boundary-Layer Shape Factor Distribution, Flat Nose Body, Re = 10^8.

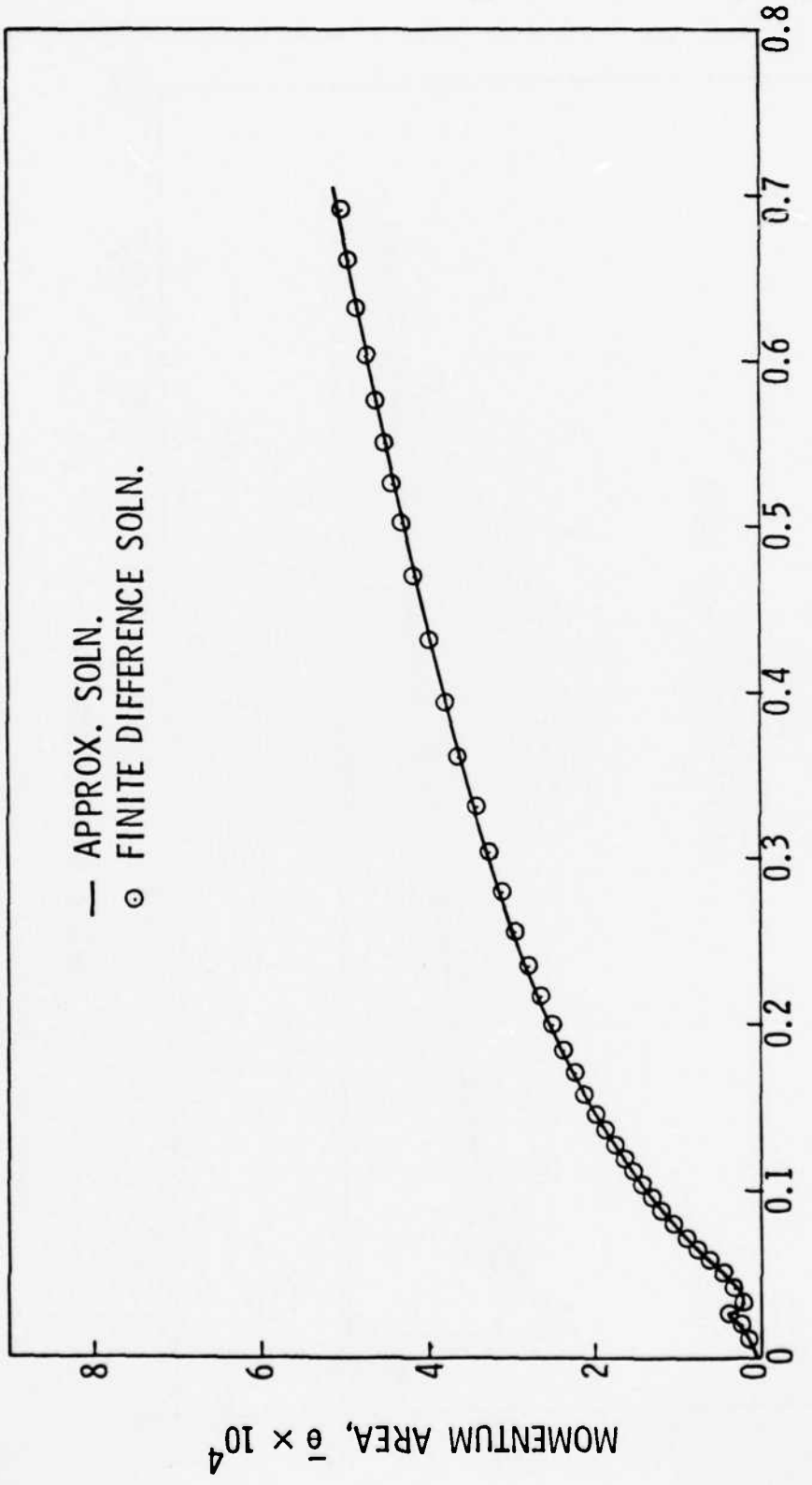

Figure 30. Boundary-Layer Momentum Area Distribution, Flat Nose Body, Re = 10^6.

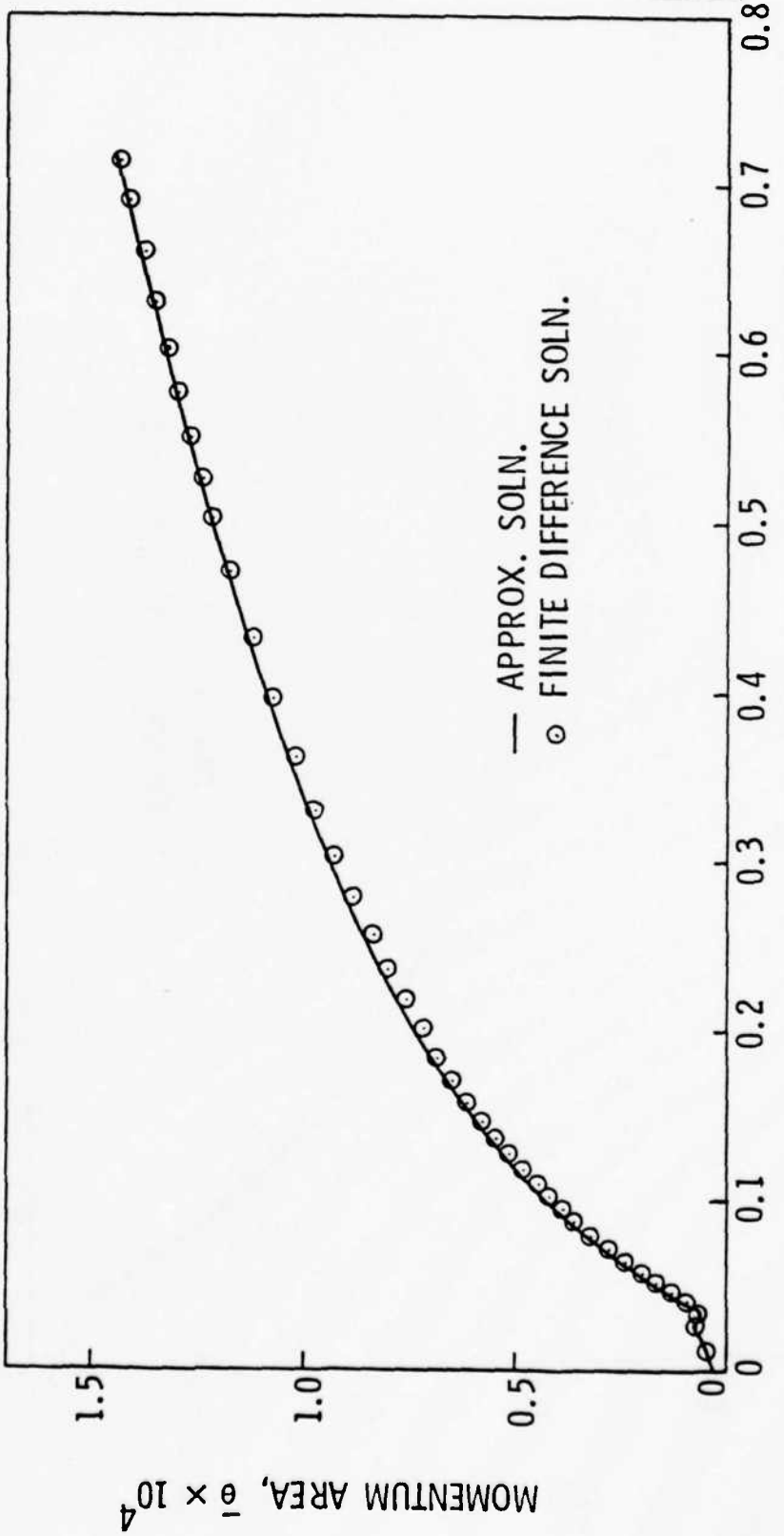

Figure 31. Boundary-Layer Momentum Area Distribution, Flat Nose Body, Re = 10^7.

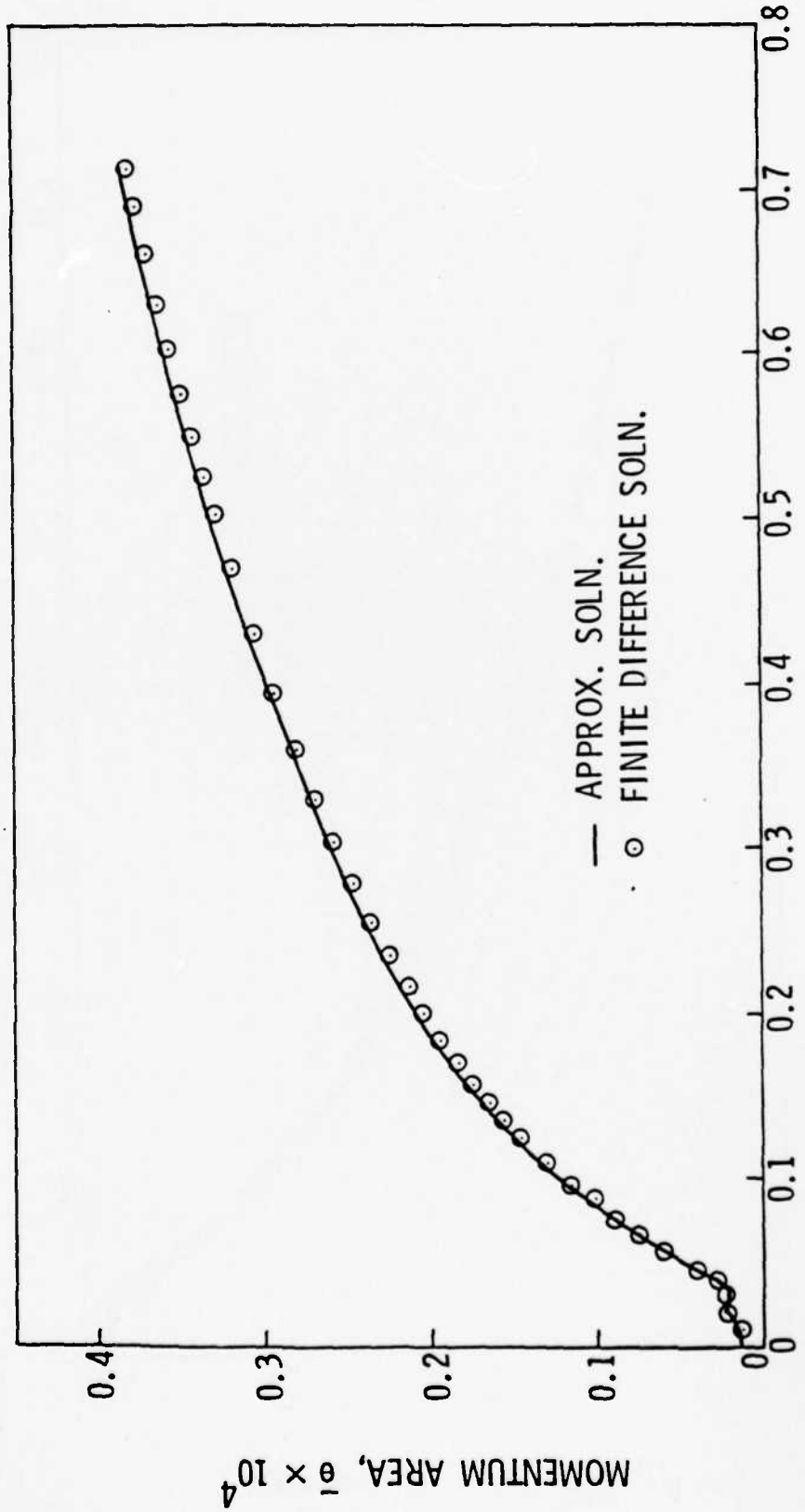

Figure 32. Boundary-Layer Momentum Area Distribution, Flat Nose Body, Re = 10^8.

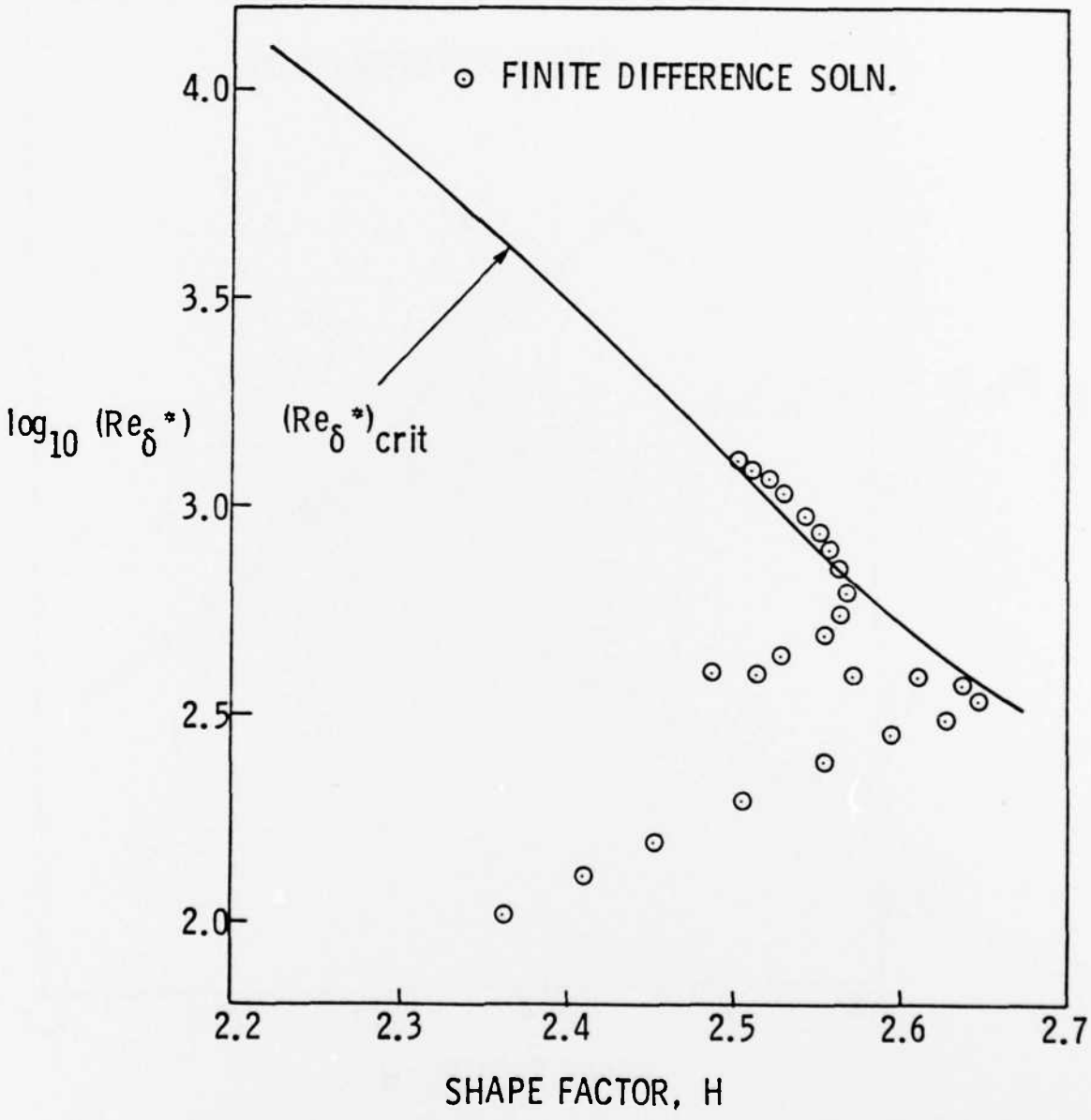

Figure 33. Path of Boundary-Layer Development, log (Re_δ^*) vs. H, Flat Nose Body, Re = 10^6.

--

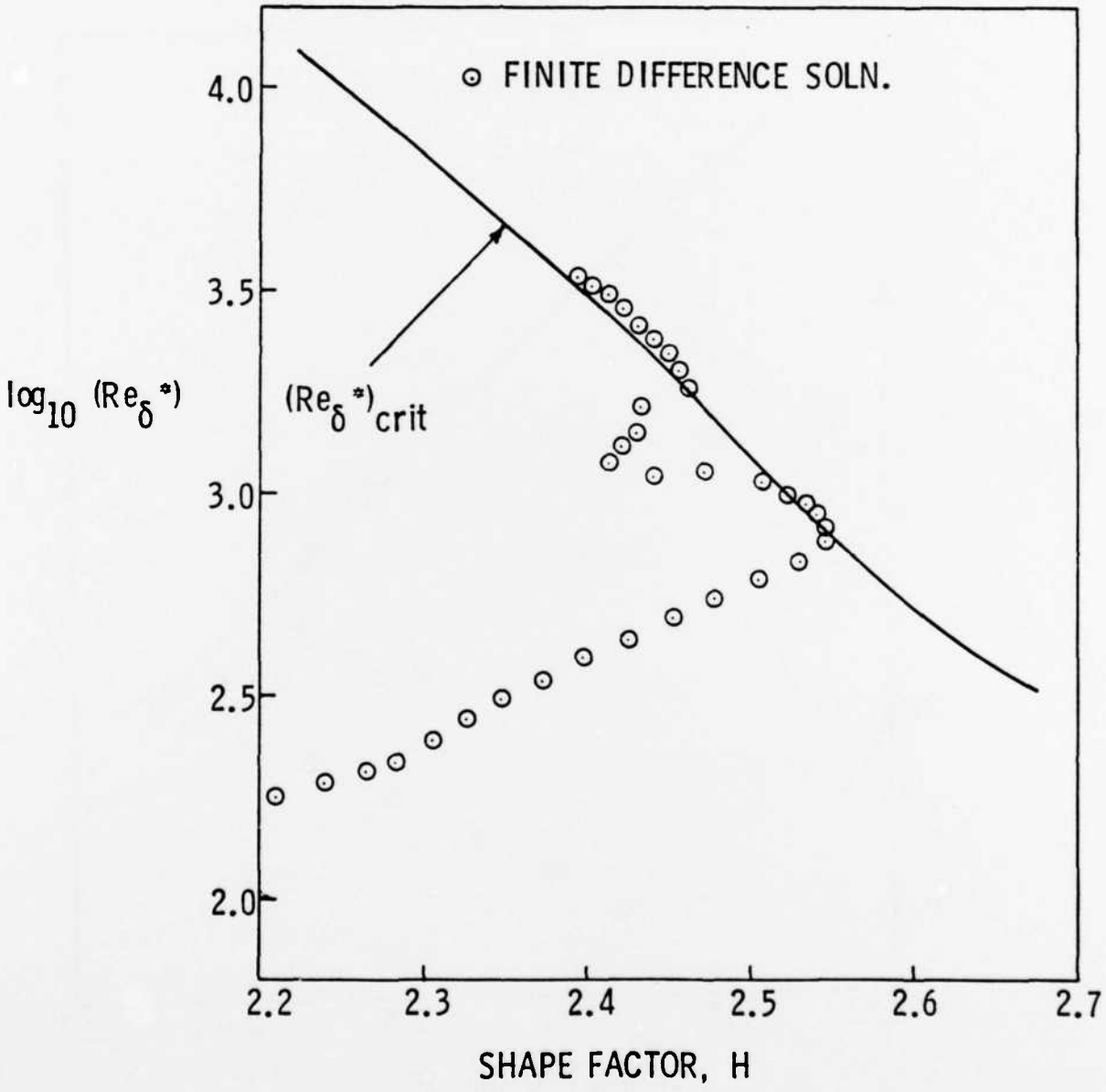

Figure 34. Path of Boundary-Layer Development, log (Re_δ^*) vs. H, Flat Nose Body, Re = 10^7.

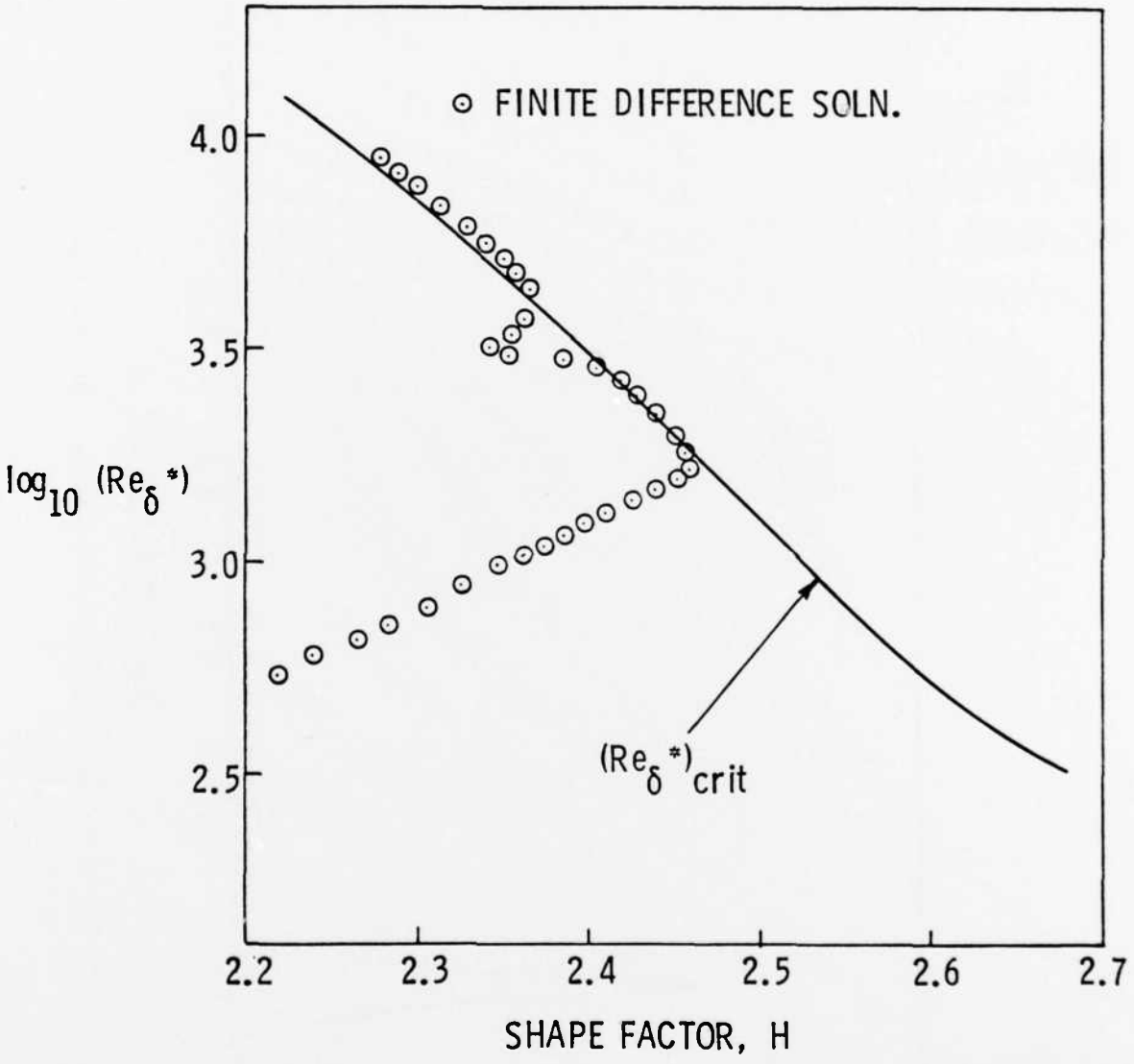

Figure 35. Path of Boundary-Layer Development, log (Re_δ*) vs. H, Flat Nose Body, Re = 10^8.

9 December 1983
GHH:1hm

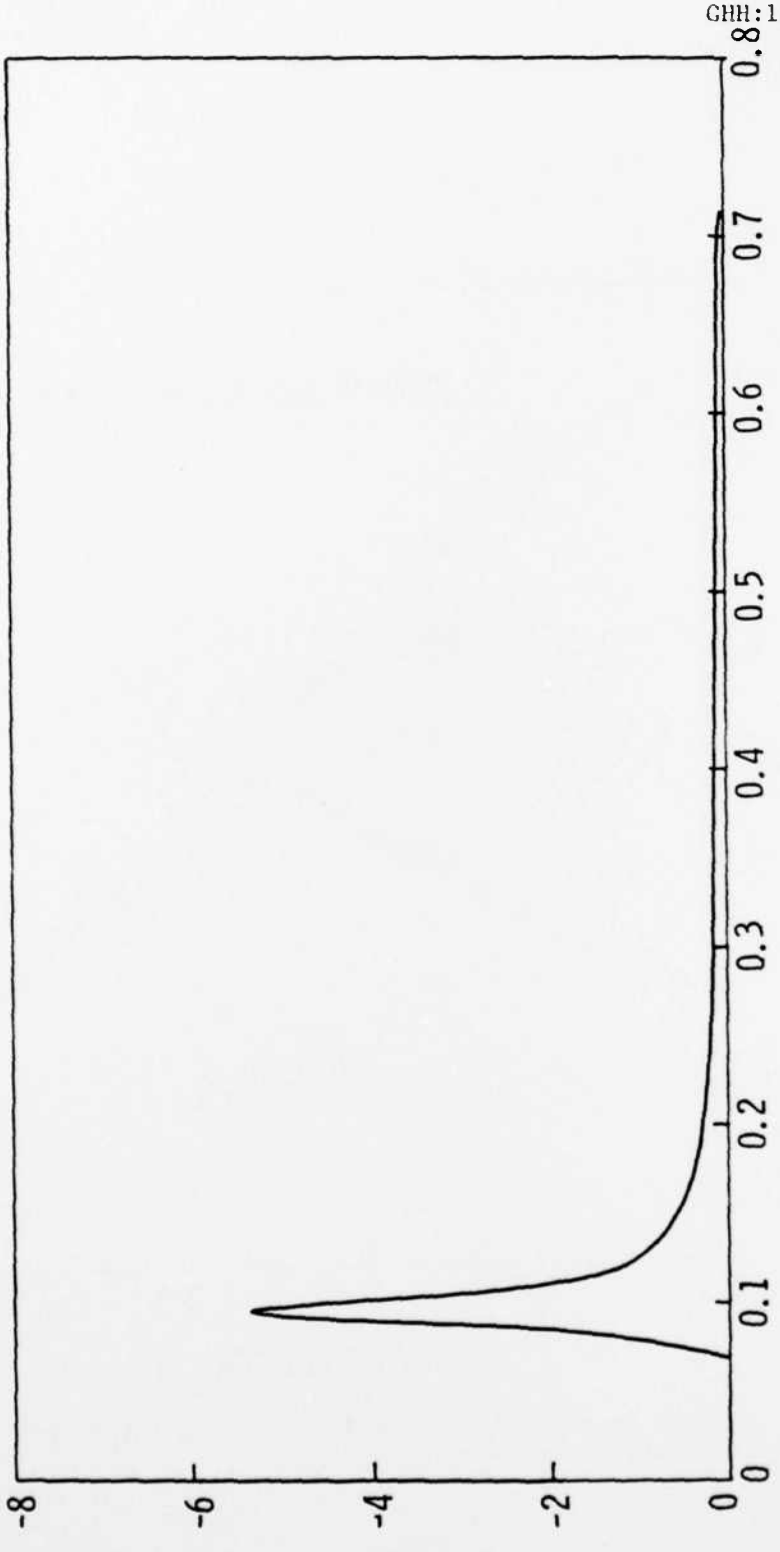

Figure 36. Suction Velocity Distribution, Flat Nose Body, Re = 10^6.

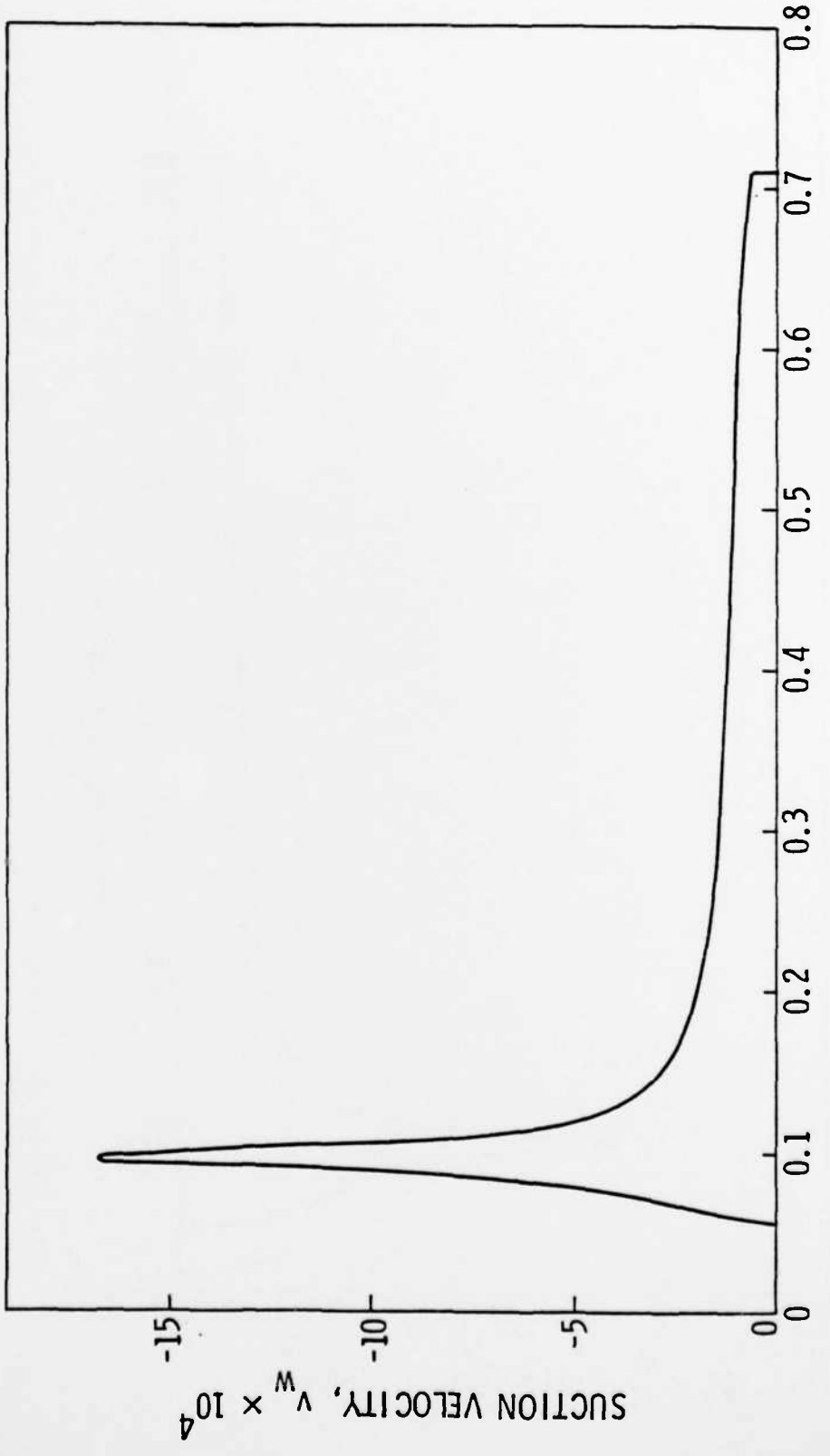

Figure 37. Suction Velocity Distribution, Flat Nose Body, Re = 10^7.

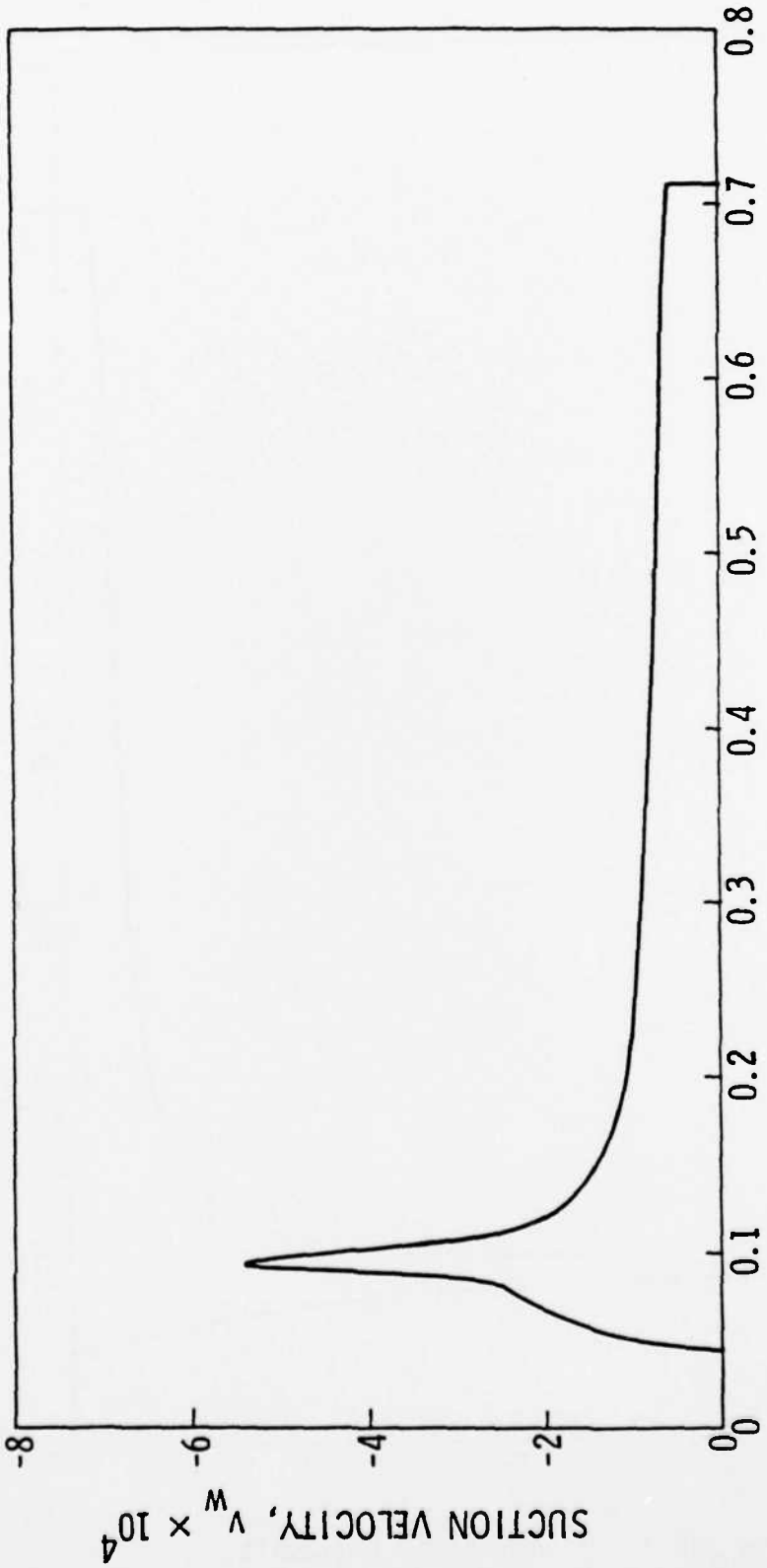

Figure 38. Suction Velocity Distribution, Flat Nose Body, Re = 10^8.

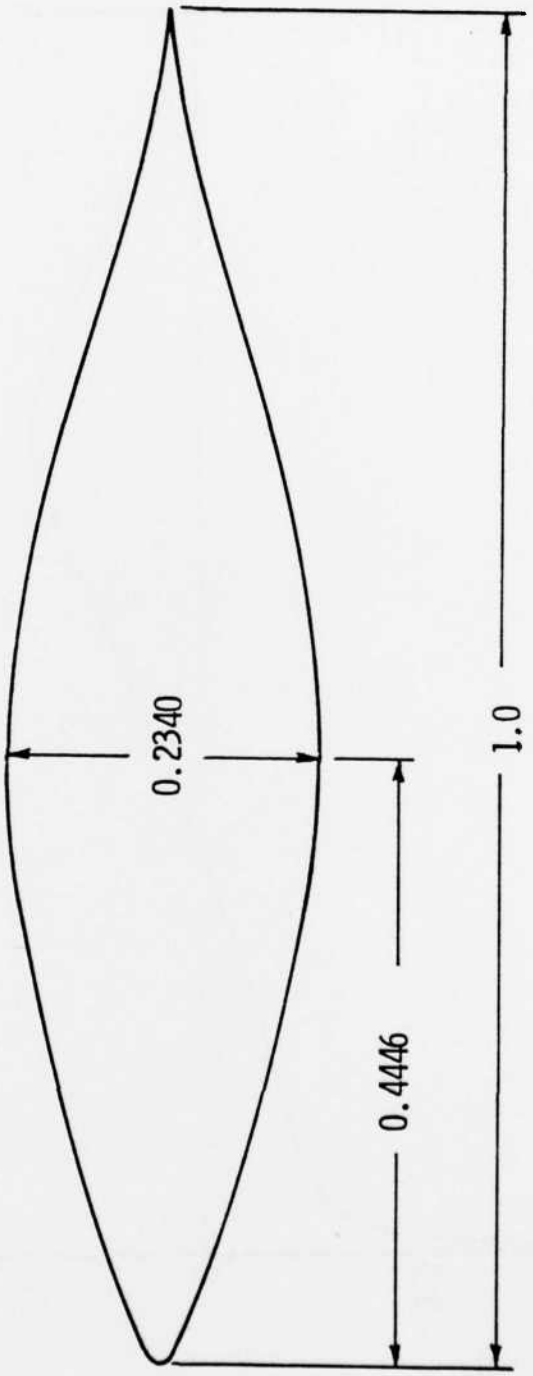

Figure 39. F-57 Body Geometry.

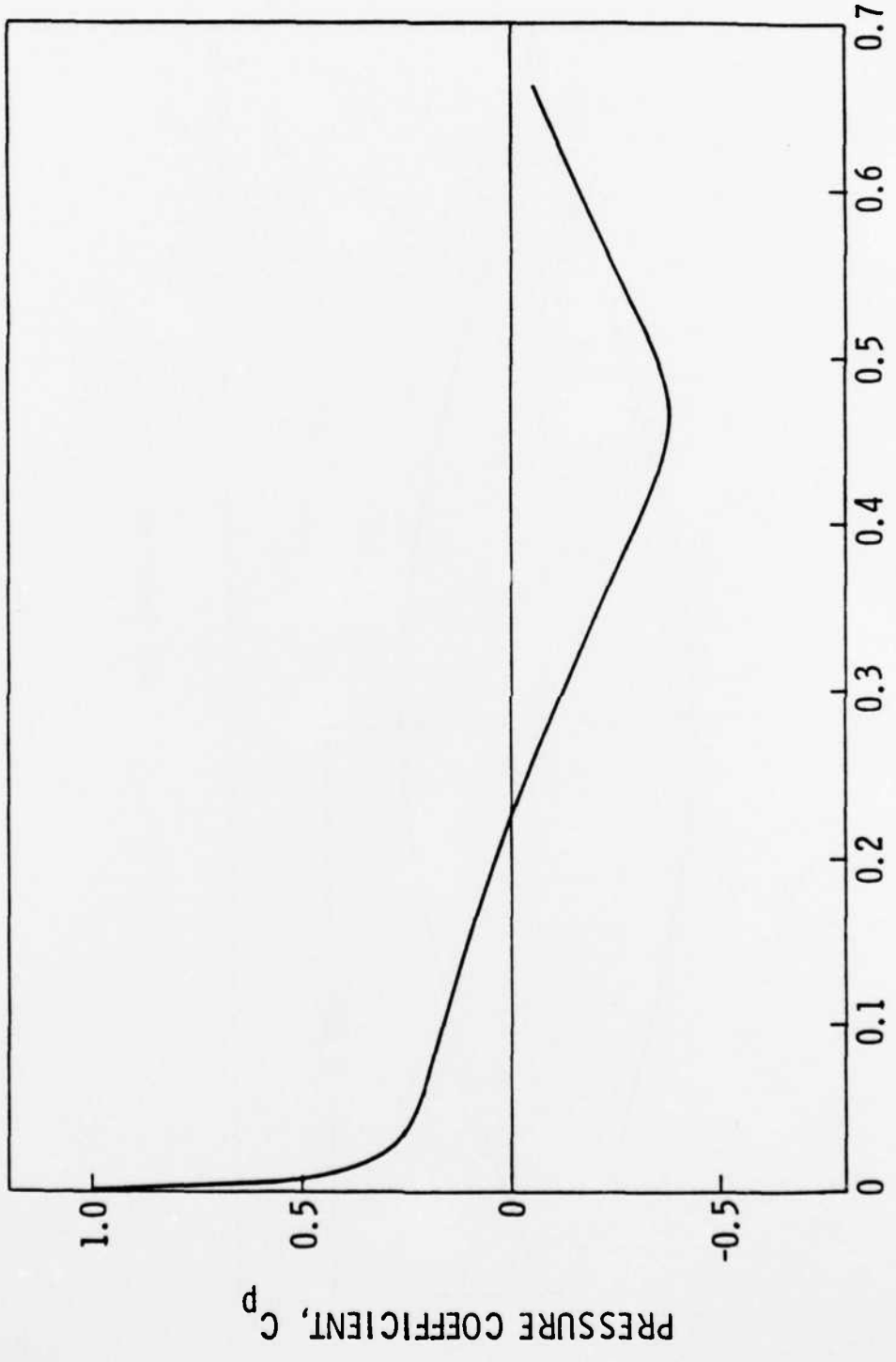

Figure 40. Pressure Distribution, F-57 Body.

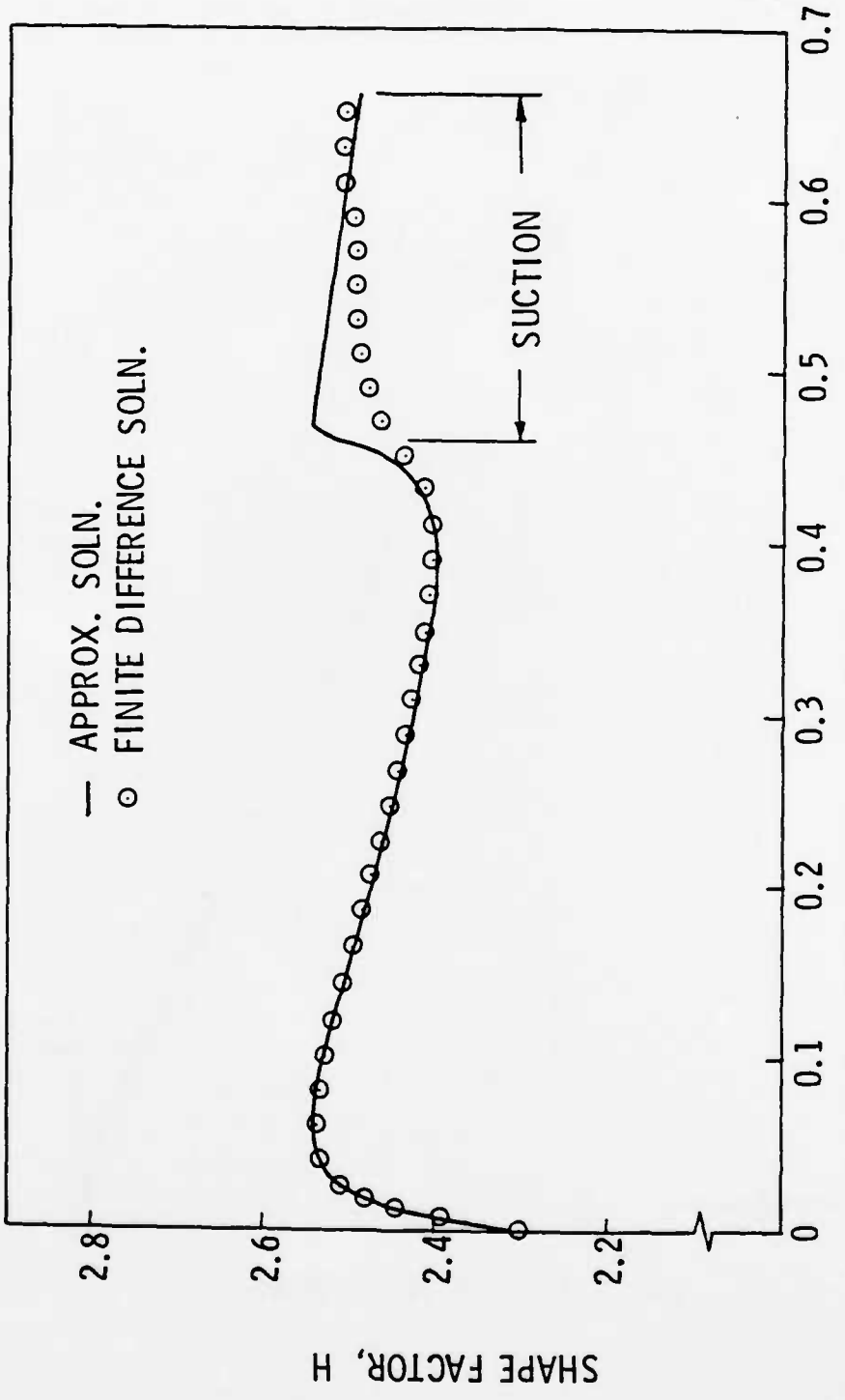

Figure 41. Boundary-Layer Shape Factor Distribution, F-57 Body, $Re = 1.2 \times 10^6$.

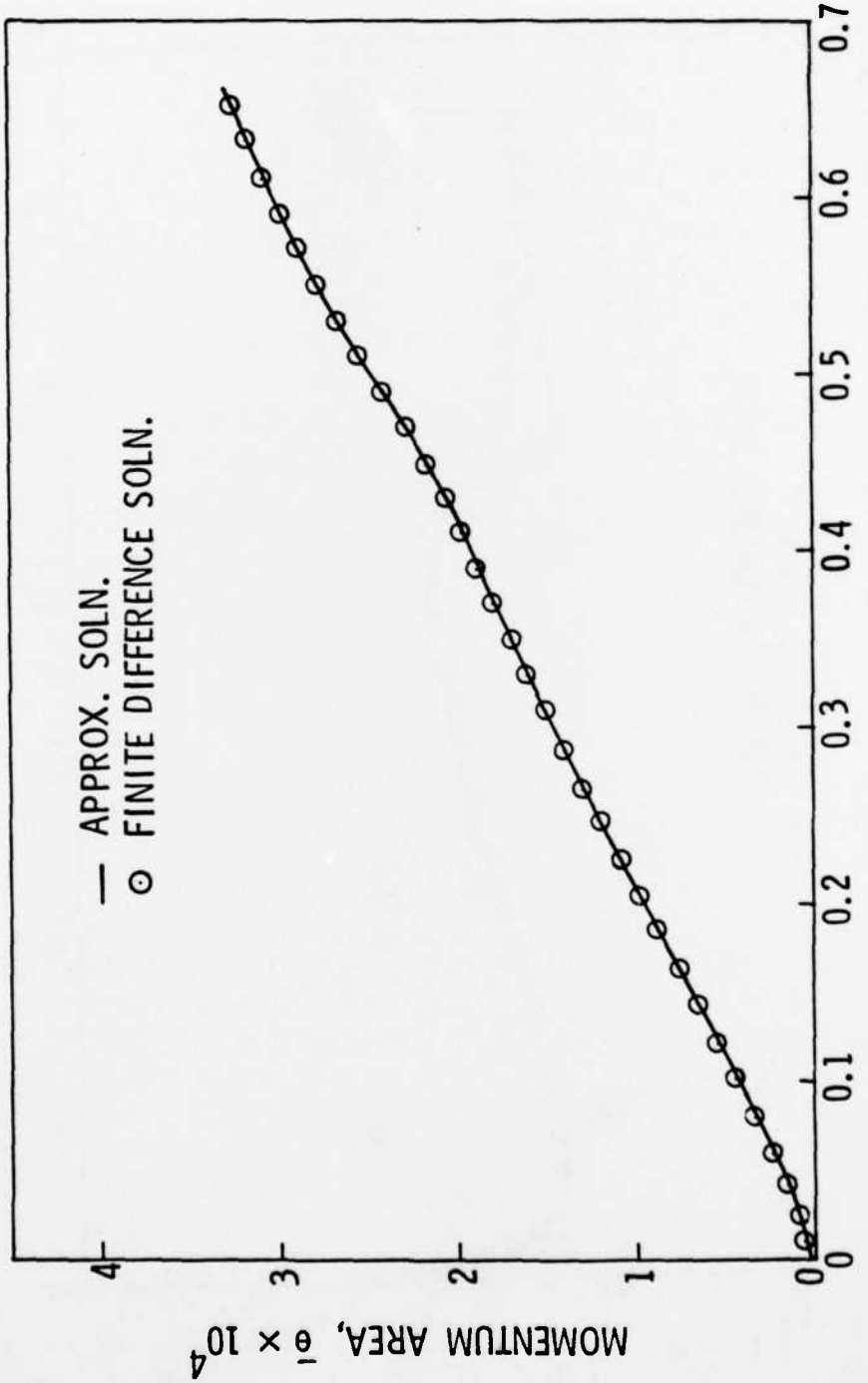

Figure 42. Boundary-Layer Momentum Area Distribution, F-57 Body, $Re = 1.2 \times 10^6$.

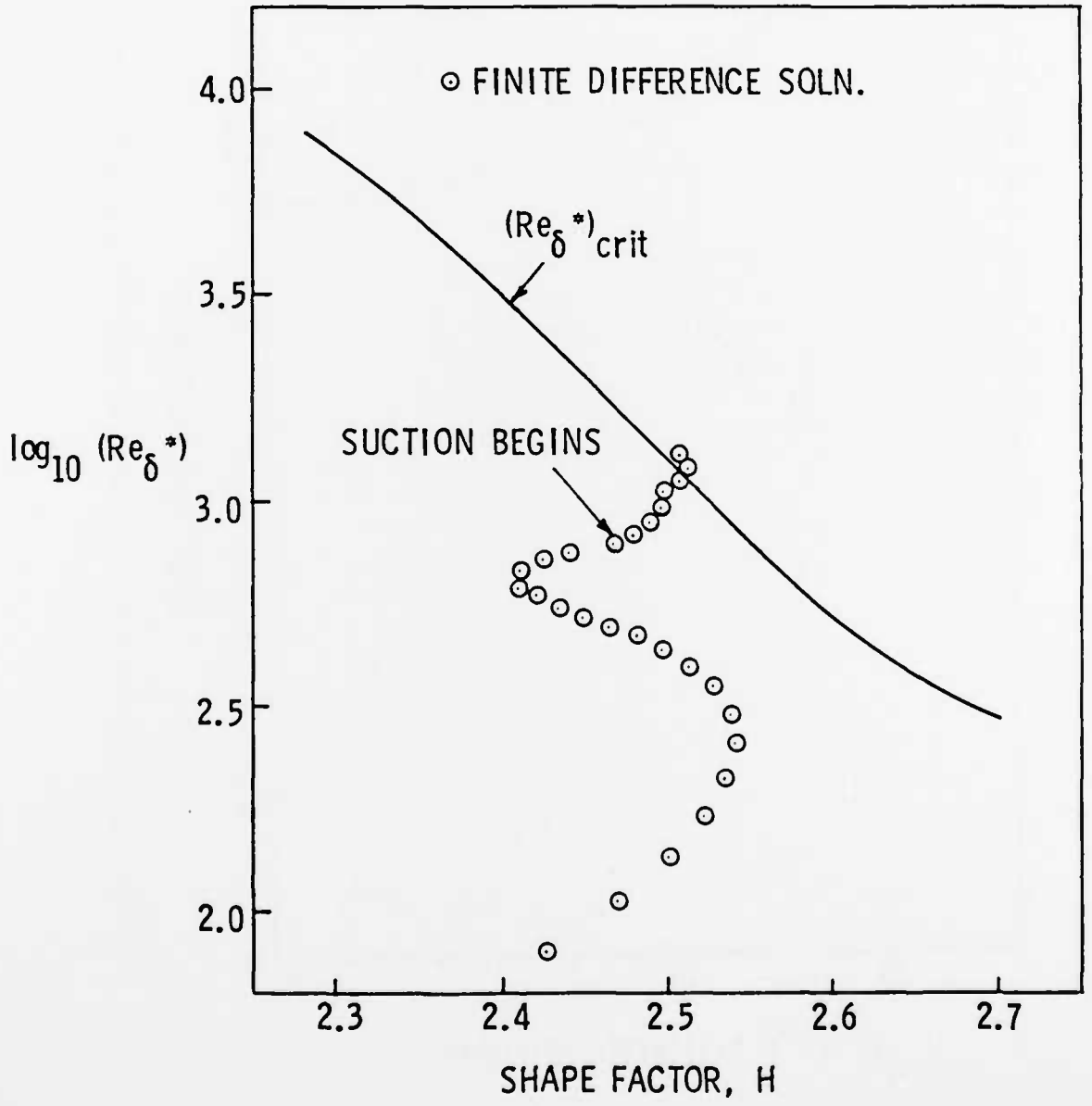

Figure 43. Path of Boundary-Layer Development, log ($Re_\delta{}^*$) vs. H, F-57 Body, Re = 1.2×10^6.

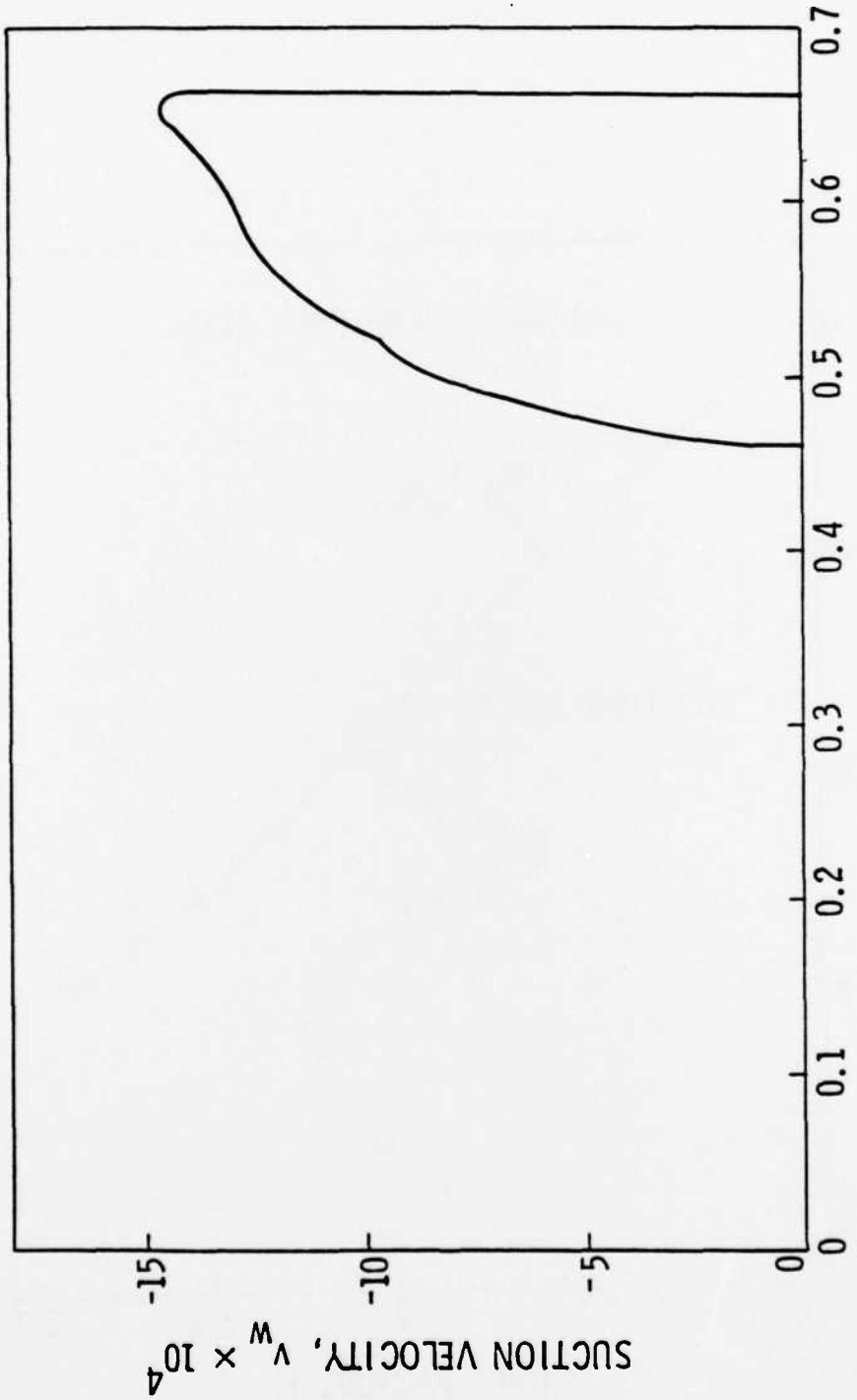

Figure 44. Suction Velocity Distribution, F-57 Body, Re = 1.2×10^6.

DISTRIBUTION LIST FOR UNCLASSIFIED TM 83-201
by G. H. Hoffman, dated 9 December 1983

Office of Naval Research
Department of the Navy
800 North Quincy Street
Arlington, VA 22217
Attn: R. E. Whitehead
(Copy No. 1)

Office of Naval Research
Department of the Navy
800 North Quincy Street
Arlington, VA 22217
Attn: C. Lee
(Copy No. 2)

Commander
Naval Sea Systems Command
Department of the Navy
Washington, DC 20362
Attn: T. E. Peirce
Code NSEA-63R31
(Copy No. 3)

Commander
Naval Underwater Systems Center
Department of the Navy
Newport, RI 02840
Attn: D. J. Goodrich
Code 3634
(Copy No. 4)

Commander
David W. Taylor Naval Ship R&D Center
Department of the Navy
Bethesda, MD 20084
Attn: Library
(Copy No. 5)

Commander
Naval Surface Weapons Center
Department of the Navy
Silver Spring, MD 20910
Attn: Library
(Copy No. 6)

Defense Technical Information Center
5010 Duke Street
Cameron Station
Alexandria, VA 22314
(Copies 7 through 12)

Naval Research Laboratory
Department of the Navy
Washington, DC 20390
Attn: Library
(Copy No. 13)

Superintendent
Code 1424
Naval Post Graduate School
Monterey, CA 93949
(Copy No. 14)

Mr. Bruce Carmichael
34795 Camino Capistrano
Capistrano Beach, CA 92624
(Copy No. 15)

Director
Applied Research Laboratory
The Pennsylvania State University
Post Office Box 30
State College, PA 16804
Attn: S. A. Abdallah
(Copy No. 16)

Director
Applied Research Laboratory
The Pennsylvania State University
Post Office Box 30
State College, PA 16804
Attn: R. J. Dopkin
(Copy No. 17)

Director
Applied Research Laboratory
The Pennsylvania State University
Post Office Box 30
State College, PA 16804
Attn: J. J. Eisenhuth
(Copy No. 18)

Director
Applied Research Laboratory
The Pennsylvania State University
Post Office Box 30
State College, PA 16804
Attn: W. S. Gearhart
(Copy No. 19)

Director
Applied Research Laboratory
The Pennsylvania State University
Post Office Box 30
State College, PA 16804
Attn: W. R. Hall
(Copy No. 20)

Director
Applied Research Laboratory
The Pennsylvania State University
Post Office Box 30
State College, PA 16804
Attn: R. E. Henderson
(Copy No. 21)

Director
Applied Research Laboratory
The Pennsylvania State University
Post Office Box 30
State College, PA 16804
Attn: G. H. Hoffman
(Copy No. 22)

Director
Applied Research Laboratory
The Pennsylvania State University
Post Office Box 30
State College, PA 16804
Attn: K. C. Kaufman
(Copy No. 23)

Director
Applied Research Laboratory
The Pennsylvania State University
Post Office Box 30
State College, PA 16804
Attn: P. H. Kurtz
(Copy No. 24)

Director
Applied Research Laboratory
The Pennsylvania State University
Post Office Box 30
State College, PA 16804
Attn: M. W. McBride
(Copy No. 25)

Director
Applied Research Laboratory
The Pennsylvania State University
Post Office Box 30
State College, PA 16804
Attn: G. C. Lauchle
(Copy No. 26)

Director
Applied Research Laboratory
The Pennsylvania State University
Post Office Box 30
State College, PA 16804
Attn: B. R. Parkin
(Copy No. 27)

Director
Applied Research Laboratory
The Pennsylvania State University
Post Office Box 30
State College, PA 16804
Attn: Garfield Thomas Water Tunnel
Files
(Copy No. 28)


ATE
LME